Inorganic Chemistry

Article

pubs.acs.org/IC

Synthesis and Electrochemical Studies of Cobalt(III) Monohydride Complexes Containing Pendant Amines

Eric S. Wiedner,*[,‡] John A. S. Roberts,[‡] William G. Dougherty,[†] W. Scott Kassel,[†] Daniel L. DuBois,[‡] and R. Morris Bullock*[,‡]

[‡]Physical Sciences Division, Pacific Northwest National Laboratory, P.O. Box 999, K2-57, Richland, Washington 99352, United States

[†]Department of Chemistry, Villanova University, 800 East Lancaster Avenue, Villanova, Pennsylvania 19085, United States

Supporting Information

ABSTRACT: Two new tetraphosphine ligands, $P^{nC\text{-}PPh_2}{}_2N^{Ph}{}_2$ (1,5-diphenyl-3,7-bis((diphenylphosphino)alkyl)-1,5-diaza-3,7-diphosphacyclooctane; alkyl = $(CH_2)_2$, n = 2 (L2); $(CH_2)_3$, n = 3 (L3)), have been synthesized. Coordination of these ligands to cobalt affords the complexes $[Co^{II}(L2)(CH_3CN)]^{2+}$ and $[Co^{II}(L3)(CH_3CN)]^{2+}$, which are reduced by KC_8 to afford $[Co^{I}(L2)(CH_3CN)]^{+}$ and $[Co^{I}(L3)(CH_3CN)]^{+}$. Protonation of the Co^{I} complexes affords $[HCo^{III}(L2)(CH_3CN)]^{2+}$ and $[HCo^{III}(L3)(CH_3CN)]^{2+}$. The cyclic voltammetry of $[HCo^{III}(L2)(CH_3CN)]^{2+}$, analyzed using digital simulation, is consistent with an $E_rC_rE_r$ reduction mechanism involving reversible acetonitrile dissociation from $[HCo^{II}(L2)(CH_3CN)]^{+}$ and resulting in formation of $HCo^{I}(L2)$. Reduction of HCo^{III} also results in cleavage of the H−Co bond from HCo^{II} or HCo^{I}, leading to formation of the Co^{I} complex $[Co^{I}(L2)(CH_3CN)]^{+}$. Under voltammetric conditions, the reduced cobalt hydride reacts with a protic solvent impurity to generate H_2 in a monometallic process involving two electrons per cobalt. In contrast, under bulk electrolysis conditions, H_2 formation requires only one reducing equivalent per $[HCo^{III}(L2)(CH_3CN)]^{2+}$, indicating a bimetallic route wherein two cobalt hydride complexes react to form 2 equiv of $[Co^{I}(L2)(CH_3CN)]^{+}$ and 1 equiv of H_2. These results indicate that both HCo^{II} and HCo^{I} can be formed under electrocatalytic conditions and should be considered as potential catalytic intermediates.

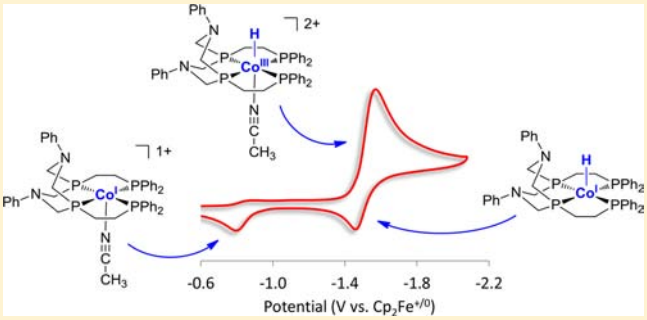

INTRODUCTION

As the use of renewable energy sources becomes more widespread, conversion of electricity into chemical bonds will become increasingly important to store the energy produced by intermittent power sources such as solar and wind.[1,2] The H−H bond of H_2 is the simplest chemical bond, but H_2 production and oxidation will require inexpensive catalysts to be economically attractive on a large scale. A wide range of molecular cobalt complexes have been reported for electrocatalytic H_2 production.[3−11] In particular, cobaloxime (**1**) and other related cobalt tetraimine complexes have been estimated to operate at overpotentials as low as 100 mV or less.[12−20] Cobalt complexes have also been studied as photocatalysts for production of H_2.[10,11,21−31]

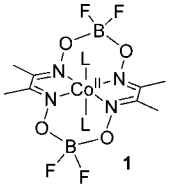

1

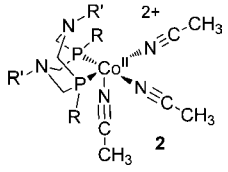

2

Formation of a Co^{III} monohydride intermediate, hereafter designated HCo^{III}, is typically invoked as a catalytic intermediate, yet the high reactivity of catalytically active HCo^{III} intermediates often precludes their experimental characterization.[3,16,32−35] Two HCo^{III} complexes containing a tetraamine ligand motif have been isolated: $HCo^{III}(dmgH)_2(P^nBu_3)$ (dmgH = dimethylglyoximate)[36,37] and $[HCo^{III}(tmen)(OH_2)]^{2+}$ (tmen = 2,3-dimethylbutane-2,3-diamine),[38] though neither of these complexes have been reported to form H_2 electrocatalytically. Recent reports have indicated that electrochemical reduction of $HCo^{III}(HMP)(CH_3CN)$ (HMP = hangman porphyrin)[6] and $[HCo^{III}(triphos)(CH_3CN)_2]^{2+}$ (triphos = $CH_3C(CH_2CH_2PPh_2)_3$)[7] in the presence of strong acids leads to electrocatalytic H_2 production, though these HCo^{III} complexes were generated in situ and have not been studied under noncatalytic conditions, that is, in the absence of acid.

We have reported cobalt complexes having a single bidentate $P^R{}_2N^{R'}{}_2$ ligand (P_2N_2 = 1,5-diaza-3,7-diphosphacyclooctane), $[Co^{II}(P^R{}_2N^{R'}{}_2)(CH_3CN)_3]^{2+}$ (**2**), that catalyze the formation of H_2 at overpotentials of 160−280 mV with turnover frequencies of 90−160 s^{-1}.[39,40] These compounds undergo ligand exchange to afford $[Co(P^R{}_2N^{R'}{}_2)_2(CH_3CN)]^{n+}$ complexes containing two

Received: May 16, 2013
Published: August 14, 2013

   dx.doi.org/10.1021/ic401232g | Inorg. Chem. 2013, 52, 9975−9988

$P^{R}{}_{2}N^{R'}{}_{2}$ ligands at either the Co^{II} oxidation state (R = R′ = Ph)[40] or the Co^{I} oxidation state (R = ^{t}Bu, R′ = Ph).[41] Accordingly no HCo^{III} species containing a single $P^{R}{}_{2}N^{R'}{}_{2}$ ligand has been isolated for this class of catalysts. We report here the synthesis of new tetradentate phosphine ligands built around a P_2N_2 moiety. Cobalt complexes bearing these ligands do not undergo ligand exchange, and they afford isolable HCo^{III} species that are structural analogs of the intermediates proposed to form during H_2 production by $[Co^{II}(P^{R}{}_{2}N^{R'}{}_{2})(CH_3CN)_3]^{2+}$. The electrochemistry of these hydride complexes under noncatalytic conditions provides insight into the redox behavior of these compounds and pathways of H_2 formation from the reduced hydride species. These reduced cobalt hydrides are important intermediates for electrocatalytic H_2 production; their catalytic performance will be detailed in a subsequent paper.

RESULTS

Synthesis and Characterization of Ligands and Complexes. The new tetradentate ligands were prepared from the asymmetric diphosphines $Ph_2P(CH_2)_2PH_2$ and $Ph_2P(CH_2)_3PH_2$.[42,43] Treatment of these terminal phosphines with 10 equiv of paraformaldehyde afforded the desired bis(hydroxymethyl)phosphines (eq 1). Subsequent treatment

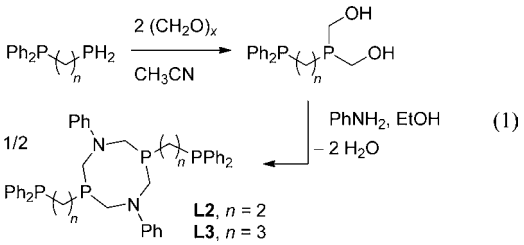

(1)

of these compounds with 1 equiv of aniline in hot acetonitrile afforded the ligands L2 and L3, where the number denotes the length of the alkyl chain linking the terminal phosphines to the cyclic phosphines. These ligands were characterized by ^{1}H and $^{31}P\{^{1}H\}$ NMR spectroscopy and elemental analysis, and the data are consistent with the assigned structures. Full experimental details and characterization are given in the Experimental Section.

Treatment of L2 with 1 equiv of $[Co^{II}(CH_3CN)_6](BF_4)_2$ in CH_3CN affords $[Co^{II}(L2)(CH_3CN)](BF_4)_2$, as shown in eq 2.

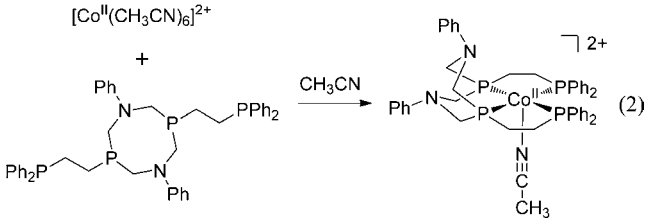

(2)

The complex $[Co^{II}(L3)(CH_3CN)](BF_4)_2$, with a $(CH_2)_3$ linker, was obtained in a similar fashion when L3 was used as the ligand. Magnetic moments of 2.30 and 2.20 μ_B were determined for $[Co^{II}(L2)(CH_3CN)]^{2+}$ and $[Co^{II}(L3)(CH_3CN)]^{2+}$, respectively, using the Evans method. These values are consistent with low-spin Co^{II} complexes with one unpaired spin.

Reduction of $[Co^{II}(L2)(CH_3CN)]^{2+}$ with KC_8 afforded the Co^{I} complex $[Co^{I}(L2)(CH_3CN)]^{+}$, as shown in eq 3. The isolated complex contained 0.5 equiv of the KBF_4 byproduct as

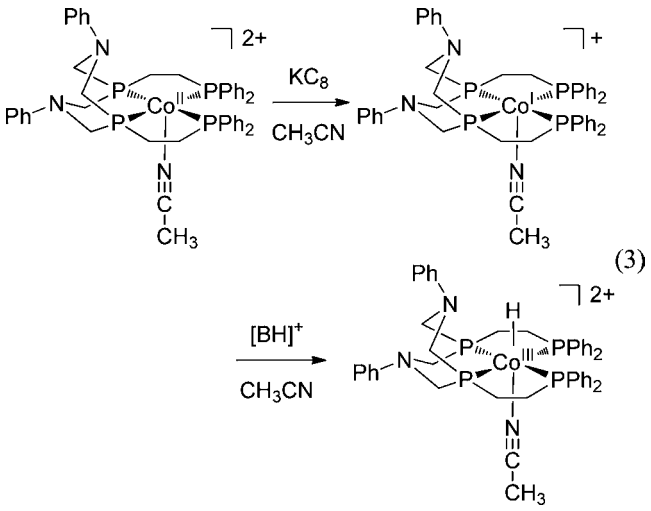

(3)

determined by integration of the ^{1}H and ^{19}F NMR spectra relative to NBu_4PF_6 that was added as an internal reference, and elemental analysis was in agreement with this formulation. Acetonitrile solutions of $[Co^{I}(L2)(CH_3CN)]^{+}$ are orange, but THF solutions of this complex are deep purple. An orange solution is obtained again if the THF solvent is removed and the product is redissolved in acetonitrile. This solvent-dependent color change suggests that the CH_3CN ligand of $[Co^{I}(L2)(CH_3CN)]^{+}$ is weakly bound, and in THF solution, a four-coordinate species, $[Co^{I}(L2)]^{+}$, is formed upon loss of the acetonitrile ligand. Only two PCH_2N resonances are observed in the ^{1}H NMR spectrum of $[Co^{I}(L2)(CH_3CN)]^{+}$ in CD_3CN, which indicates that each face of the L2 ligand is equivalent on the NMR time scale and that the acetonitrile ligand is exchanging rapidly. Two broad doublets are observed at 77.1 and 73.5 ppm in the $^{31}P\{^{1}H\}$ NMR spectrum of $[Co^{I}(L2)(CH_3CN)]^{+}$. This splitting pattern is consistent with an AA′BB′ spectrum that is broadened due to coupling between phosphorus and the quadrupolar ^{59}Co nucleus (I = 7/2, 100%). The complex $[Co^{I}(L3)(CH_3CN)]^{+}$ can be generated in a similar manner, with $^{31}P\{^{1}H\}$ NMR resonances shifted upfield to 20.1 and 11.2 ppm. This 60 ppm upfield shift results from the expansion of the chelate rings formed by the linker arms from five to six atoms.[44]

Protonation of *in situ* generated $[Co^{I}(L2)(CH_3CN)]^{+}$ with *p*-bromoanilinium tetrafluoroborate affords the hydride complex $[HCo^{III}(L2)(CH_3CN)]^{2+}$ (eq 3), which can be separated from the KBF_4 byproduct by extraction with CH_2Cl_2. The hydride complex is indefinitely stable in the solid state and in acetonitrile solution at room temperature under N_2. Isolated $[HCo^{III}(L2)(CH_3CN)]^{2+}$ typically contains small amounts (<10%) of $[Co^{II}(L2)(CH_3CN)]^{2+}$ as determined by ^{1}H NMR spectroscopy. The hydride resonance appears as a broad singlet at −21.2 ppm ($\Delta\nu_{1/2}$ = 144 Hz) in the ^{1}H NMR spectrum, and a resonance corresponding to the acetonitrile ligand is found at 1.75 ppm. In CD_3CN solution, the peak intensity of the coordinated acetonitrile ligand gradually diminishes over the course of days and is accompanied by a corresponding increase in the resonance for free acetonitrile at 1.96 ppm, which indicates that dissociation of the acetonitrile ligand is slow. A very broad resonance is observed in the $^{31}P\{^{1}H\}$ NMR spectrum. Lineshape analysis of this resonance reveals the presence of two broad signals at approximately 80 ($\Delta\nu_{1/2} \approx$ 930 Hz) and 76 ppm ($\Delta\nu_{1/2} \approx$ 1500 Hz); the spectrum and details of the fitting are given in the Supporting Information.

dx.doi.org/10.1021/ic401232g | Inorg. Chem. 2013, 52, 9975−9988

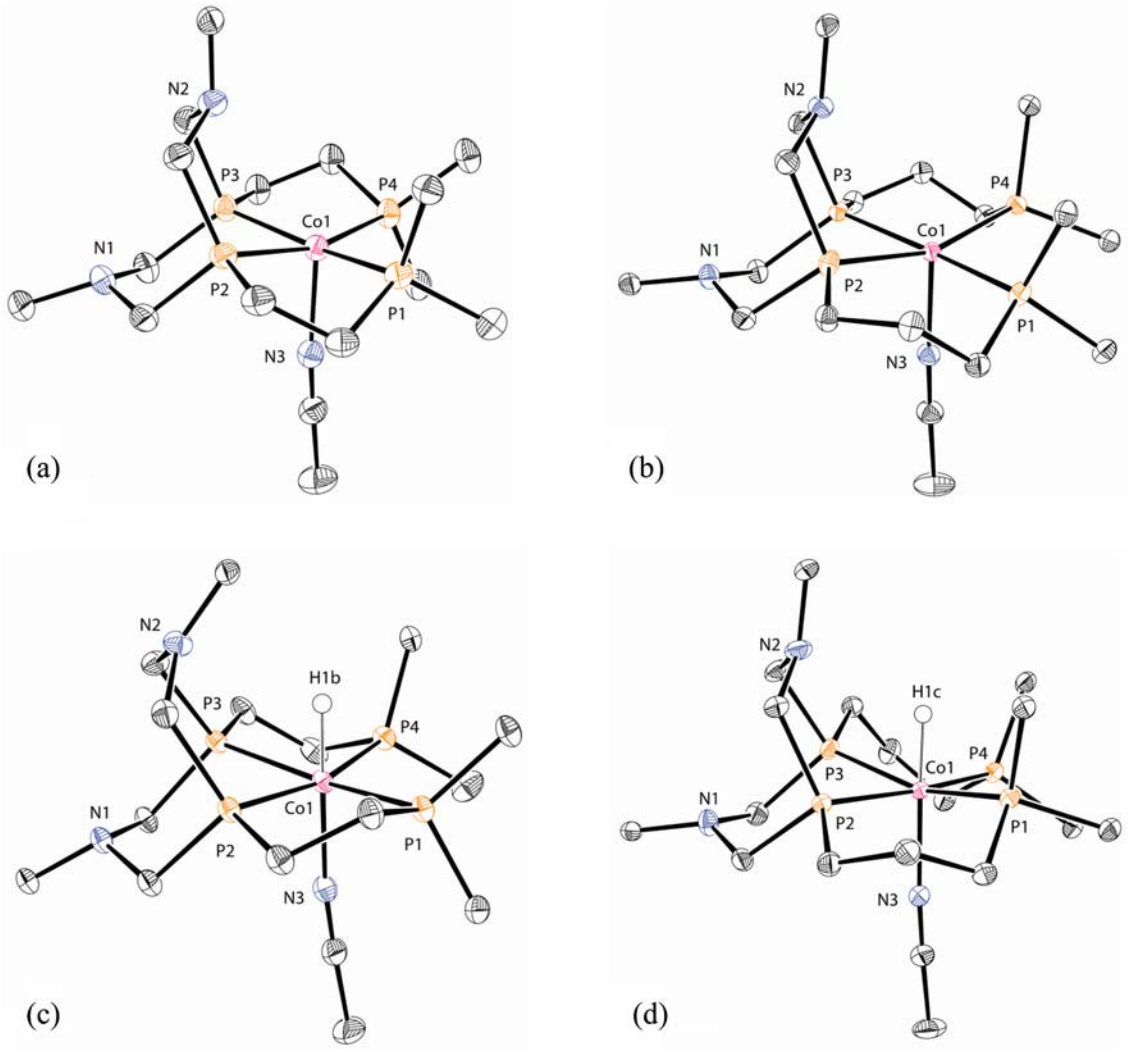

Figure 1. X-ray crystal structure diagrams of the dications of $[Co(L2)(CH_3CN)](BF_4)_2$ (a), $[Co(L3)(CH_3CN)](BF_4)_2$ (b), $[HCo(L2)(CH_3CN)](BF_4)_2$ (c), and $[HCo(L3)(CH_3CN)](BF_4)_2$ (d). All hydrogen atoms are omitted except for the hydride ligands attached to cobalt in panels c and d. Only the *ipso* carbons of the phenyl rings are shown for clarity. Thermal ellipsoids are shown at the 50% probability level.

Table 1. Selected Bond Distances (Å)

compound	Co−P(1)	Co−P(2)	Co−P(3)	Co−P(4)	Co−N(3)
$[Co^{II}(L2)(CH_3CN)]^{2+}$	2.2241(4)	2.1863(4)	2.1744(4)	2.2602(4)	2.0031(11)
$[Co^{II}(L3)(CH_3CN)]^{2+}$	2.2940(4)	2.2440(5)	2.2452(4)	2.3138(4)	2.0041(12)
$[HCo^{III}(L2)(CH_3CN)]^{2+}$	2.2329(4)	2.1805(4)	2.1763(4)	2.2356(4)	1.9434(13)
$[HCo^{III}(L3)(CH_3CN)]^{2+}$	2.2746(4)	2.2267(4)	2.1982(4)	2.2697(4)	1.9444(11)

The hydride complex $[HCo^{III}(L3)(CH_3CN)]^{2+}$ can be prepared in a similar manner. The hydride resonance of $[HCo^{III}(L3)(CH_3CN)]^{2+}$ appears as a pentet at −19.66 ppm ($^2J_{HP}$ = 46.7 Hz), which is in contrast to the broad singlet observed for the hydride resonance of $[HCo^{III}(L2)(CH_3CN)]^{2+}$. Additionally, the $^{31}P\{^1H\}$ NMR spectrum of $[HCo^{III}(L3)(CH_3CN)]^{2+}$ displays resonances at 21.8 ppm ($\Delta\nu_{1/2}$ = 234 Hz) and 18.4 ppm ($\Delta\nu_{1/2}$ = 211 Hz) that are much narrower than those observed for $[HCo^{III}(L2)(CH_3CN)]^{2+}$. These differences in the NMR line widths suggest that quadrupolar relaxation of the hydrogen and phosphorus atoms bound to cobalt is more efficient in $[HCo^{III}(L3)(CH_3CN)]^{2+}$ than in $[HCo^{III}(L2)(CH_3CN)]^{2+}$.

Structural Studies. Crystals of $[Co^{II}(L2)(CH_3CN)]^{2+}$, $[Co^{II}(L3)(CH_3CN)]^{2+}$, $[HCo^{III}(L2)(CH_3CN)]^{2+}$, and $[HCo^{III}(L3)(CH_3CN)]^{2+}$ suitable for X-ray diffraction were grown by layering ether onto an acetonitrile solution of each complex. A drawing of each cation is shown in Figure 1, and selected bond distances and angles are given in Table 1 and Table S2, Supporting Information. The structure of $[Co^{II}(L2)(CH_3CN)]^{2+}$ has a square pyramidal geometry with the four phosphorus atoms of the L2 ligand occupying the basal positions and an acetonitrile ligand occupying the axial position. One six-membered chelate ring of the cyclic P_2N_2 fragment adopts a chair conformation, minimizing steric interactions with the acetonitrile ligand, and the other six-membered ring has a boat conformation. Each arm of the L2 ligand forms a five-membered chelate ring containing one phosphorus from the cyclic P_2N_2 fragment (P_C) and one of the terminal diphenylphosphino fragments (P_T). The P(2)−Co−P(3) bite

dx.doi.org/10.1021/ic401232g | *Inorg. Chem.* 2013, 52, 9975−9988

angle of the P_2N_2 fragment (P_C–Co–P_C) is small (81.096(14)°) as typically observed for $[M^{II}(P^R{}_2N^{R'}{}_2)(CH_3CN)]^{2+}$ (M = Co, Ni) and $[Ni^{II}(P^R{}_2N^{R'}{}_2)_2(CH_3CN)]^{2+}$ complexes,[39,41,45–47] and the average P_C–Co–P_T bite angle of 85.880(20)° is typical for a five-membered diphosphine ligand. The average Co–P_C bond length of 2.1804(6) Å is shorter than the average Co–P_T bond length of 2.2422(6) Å. The structure of $[Co^{II}(L3)(CH_3CN)]^{2+}$ is very similar to that of $[Co^{II}(L2)(CH_3CN)]^{2+}$, with the major difference being the larger average P_C–Co–P_T bite angle of 90.640(22)° for $[Co^{II}(L3)(CH_3CN)]^{2+}$ due to the larger six-membered chelate ring of this complex.

The solid state structure of $[HCo^{III}(L2)(CH_3CN)]^{2+}$ is similar to that of $[Co^{II}(L2)(CH_3CN)]^{2+}$, with the exception that the hydride ligand, which was located in the difference map, occupies the sixth coordination site *trans* to the acetonitrile ligand. The Co–P bond lengths and P–Co–P bite angles of $[HCo^{III}(L2)(CH_3CN)]^{2+}$ are similar to those observed for $[Co^{II}(L2)(CH_3CN)]^{2+}$. In the structure for $[HCo^{III}(L2)(CH_3CN)]^{2+}$, the axial acetonitrile ligand has a Co(1)–N(3) bond length of 1.9434(13) Å, while the corresponding bond length in $[Co^{II}(L2)(CH_3CN)]^{2+}$ is significantly longer at 2.0031(11) Å. This is consistent with removal of an electron from the d_{z^2} orbital that is antibonding with respect to the acetonitrile ligand upon transitioning from Co^{II} to Co^{III}. As expected, the solid state structure of $[HCo^{III}(L3)(CH_3CN)]^{2+}$ is similar to that of $[HCo^{III}(L2)(CH_3CN)]^{2+}$ with the exception of the larger average P_C–Co–P_T bite angle (90.001(18)°) for $[HCo^{III}(L3)(CH_3CN)]^{2+}$.

The equatorial P atoms show a dihedral twist about the Co atom that is greater for $[HCo^{III}(L3)(CH_3CN)]^{2+}$ than for $[HCo^{III}(L2)(CH_3CN)]^{2+}$. This distortion is most evident through comparison of the two equatorial dihedral angles (α), one of which is defined by the opposing P_C–Co–P_T planes and the other by the P_C–Co–P_C and P_T–Co–P_T planes. These angles are smaller for $[HCo^{III}(L2)(CH_3CN)]^{2+}$ (11.4° and 12.3°, respectively) than for $[HCo^{III}(L3)(CH_3CN)]^{2+}$ (18.3° and 18.6°). This structural detail influences the redox properties of these complexes, as discussed below. In contrast, the dihedral angles for $[Co^{II}(L2)(CH_3CN)]^{2+}$ and $[Co^{II}(L3)(CH_3CN)]^{2+}$ are very similar (13.8–15.2°).

Electrochemical Studies. The cyclic voltammogram of $[Co^{II}(L2)(CH_3CN)]^{2+}$ in acetonitrile (Figure 2a) shows a reversible wave having a half-wave potential $E_{1/2}$ of −0.82 V vs $Cp_2Fe^{+/0}$ (the reference couple for all potentials in this paper), similar to the $Co^{II/I}$ couples of other $[Co^{II}(diphosphine)_2(CH_3CN)]^{2+}$ complexes.[48,49] The anodic and cathodic peak currents (i_{pa} and i_{pc}) show a linear dependence on the scan rate $\upsilon^{1/2}$, indicating diffusion control. An irreversible reduction wave with cathodic peak potential E_{pc} = −2.52 V and with i_{pc} roughly double that of the $Co^{II/I}$ wave is assigned to the reduction of Co^{I} to Co^{-I}. $[Co^{II}(L3)(CH_3CN)]^{2+}$ also shows a reversible $Co^{II/I}$ wave with $E_{1/2}$ = −0.82 V, and in this case shows two partially resolved irreversible reduction waves with E_{pc} = −2.20 and −2.32 V, assigned to the $Co^{I/0}$ and $Co^{0/-I}$ couples, respectively (Figure S2, Supporting Information). A small reduction wave at approximately −1.1 V is observed occasionally in voltammograms of $[Co^{II}(L2)(CH_3CN)]^{2+}$ and frequently in voltammograms of $[Co^{II}(L3)(CH_3CN)]^{2+}$; these reductions are attributed to minor coordination isomers and are discussed in more detail in the Supporting Information.

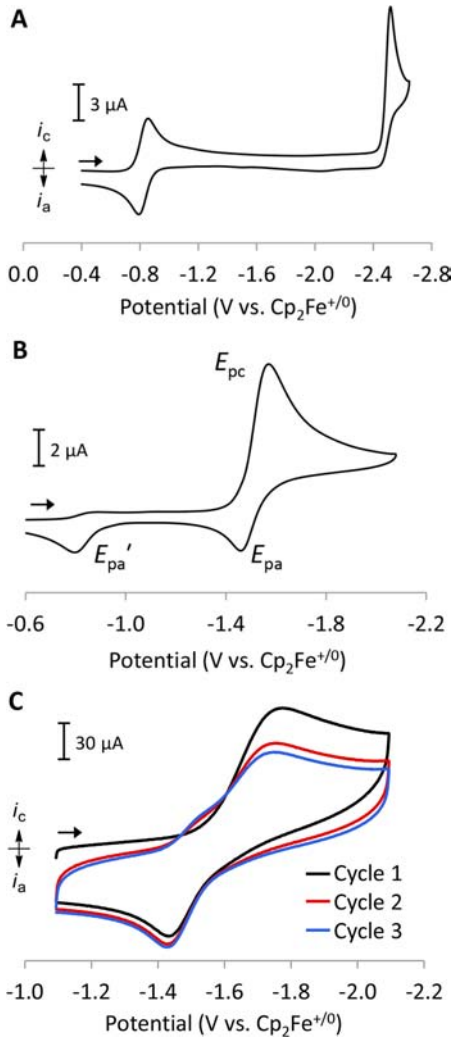

Figure 2. (A) Cyclic voltammogram of $[Co^{II}(L2)(CH_3CN)]^{2+}$ at υ = 0.1 V s^{-1}, (B) cyclic voltammogram of $[HCo^{III}(L2)(CH_3CN)]^{2+}$ at υ = 0.1 V s^{-1}, and (C) cyclic voltammograms (three cycles) of $[HCo^{III}(L2)(CH_3CN)]^{2+}$ at 50 V s^{-1}. Conditions: 2 mM analyte, 0.2 M NBu_4PF_6 acetonitrile solution, glassy carbon working electrode, 23 ± 2 °C.

Reduction of $[HCo^{III}(L2)(CH_3CN)]^{2+}$ (Figure 2b) is quasireversible at υ = 0.1 V s^{-1}, with E_{pc} = −1.57 V and E_{pa} = −1.47 V. The peak-to-peak separation (ΔE_p) of 100 mV is larger than that for $Cp_2Fe^{+/0}$ under the same conditions (68 mV; not shown). Cyclic voltammograms of $[HCo^{III}(L3)(CH_3CN)]^{2+}$ were similar in appearance, with E_{pc} = −1.29 V and E_{pa} = −1.21 V at υ = 0.1 V s^{-1} (Figure S3, Supporting Information). A linear dependence of i_{pc} on $\upsilon^{1/2}$ indicates diffusion control for reduction of $[HCo^{III}(L2)(CH_3CN)]^{2+}$ (Figure S4, Supporting Information). A new wave is observed on the return sweep at E_{pa}' = −0.80 V, where the prime (′) indicates a voltammetric property associated with this oxidation. This wave is consistent with oxidation of $[Co^{I}(L2)(CH_3CN)]^{+}$, which could be formed by net loss of either $H^{\bullet}$ or H^{-} in a H–Co bond cleavage reaction. The mechanism of the H–Co bond cleavage reaction is investigated subsequent to the following analysis of the quasireversible HCo^{III} reduction wave.

Figure 2c shows the voltammograms obtained when the applied potential was cycled three times through the $[HCo^{III}(L2)(CH_3CN)]^{2+}$ reduction wave at υ = 50 V s^{-1}. In

dx.doi.org/10.1021/ic401232g | *Inorg. Chem.* 2013, 52, 9975–9988

Scheme 1. $E_rC_rE_r$ Mechanism for Reduction of $[HCo^{III}(L2)(CH_3CN)]^{2+}$

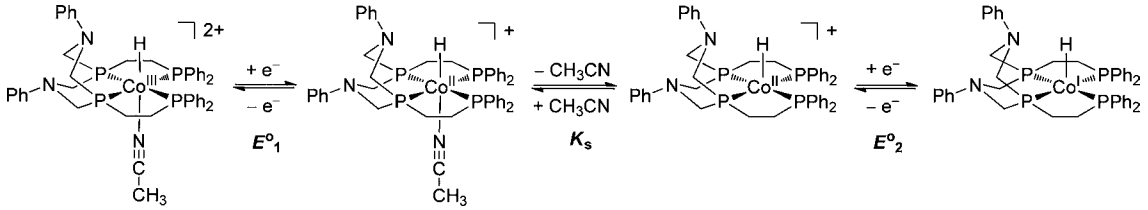

the first cycle (black trace), the peak potential for reduction of $[HCo^{III}(L2)(CH_3CN)]^{2+}$ is observed at −1.73 V, and a new shoulder appears at approximately −1.53 V on the second and third cathodic sweeps (red and blue traces). This indicates that reduction of $[HCo^{III}(L2)(CH_3CN)]^{2+}$ on the cathodic sweep followed by oxidation on the return anodic sweep does not completely regenerate $[HCo^{III}(L2)(CH_3CN)]^{2+}$. Therefore reduction of $[HCo^{III}(L2)(CH_3CN)]^{2+}$ proceeds by an $E_rC_rE_r$ mechanism having two reversible electron transfers (E_r) and an intervening reversible chemical step (C_r). We propose that the chemical step of this $E_rC_rE_r$ sequence is the reversible dissociation of CH_3CN from $[HCo^{II}(L2)(CH_3CN)]^{+}$ (Scheme 1) to form $[HCo^{II}(L2)]^{+}$. The final reduction product of this $E_rC_rE_r$ sequence is $HCo^{I}(L2)$, and the rate of formation of this complex depends on the rate at which CH_3CN dissociates from $[HCo^{II}(L2)(CH_3CN)]^{+}$. In this case, the potential of the first electron transfer to $[HCo^{III}(L2)(CH_3CN)]^{2+}$ (E_1°) is more negative than the potential of the second electron transfer to $[HCo^{II}(L2)]^{+}$ (E_2°). A similar reduction mechanism is observed for $[HCo^{III}(dppe)_2(CH_3CN)]^{2+}$, and the analogues $[HCo^{II}(dppe)_2]^{+}$ and $HCo^{I}(dppe)_2$ have been independently synthesized and characterized.[48]

With redox reactions involving chemical steps, the evolution of peak potentials with scan rate depends on the mechanism.[50,51] An ideal reversible one-electron redox reaction followed by an irreversible chemical reaction (an E_rC_i mechanism) has a characteristic slope of $\Delta E_p/\Delta\log(\upsilon) = 30$ mV. For an $E_rC_iE_r$ pathway, the peak potential changes with $\log(\upsilon)$ precisely as for the E_rC_i process.[52] Plots of experimentally measured E_{pc} values versus $\log(\upsilon)$ between $\upsilon = 0.05$ and 5 V s^{-1} afford a slope of 34 mV for $[HCo^{III}(L2)(CH_3CN)]^{2+}$ and 41 mV for $[HCo^{III}(L3)(CH_3CN)]^{2+}$ (Figure S5, Supporting Information), which supports the $E_rC_rE_r$ mechanism proposed in Scheme 1. These slopes increase to 86−89 mV with scan rates greater than $\upsilon = 5$ V s^{-1}, which is consistent with a transition from reversible to quasireversible electron transfer. Unlike E_{pc}, the slope of E_{pa} versus $\log(\upsilon)$ is only 11 mV between $\upsilon = 0.05$ and 50 V s^{-1} and can be attributed to solution resistance. This suggests that binding of acetonitrile to $[HCo^{II}(L2)]^{+}$ is slow on the voltammetry time scale; otherwise a greater variation in E_{pa} would be observed.

As mentioned above, H−Co bond cleavage can occur upon reduction of $[HCo^{III}(L2)(CH_3CN)]^{2+}$, and this process results in the formation of $[Co^{I}(L2)(CH_3CN)]^{+}$. We consider two types of mechanisms, either or both of which may be operative: a bimetallic reaction requiring one electron per Co and forming H_2 by net loss of $H^\bullet$ and a monometallic reaction requiring two electrons per Co and involving net loss of H^- to a protic solvent impurity such as H_2O. These reaction pathways are illustrated for HCo^{II} in Scheme 2, though it is important to note that the electron stoichiometry is independent of the oxidation state of the reactive cobalt hydride. In principle

Scheme 2. Mechanisms for Bimetallic and Monometallic H−Co Bond Cleavage

Bimetallic Pathway

$$2\,HCo^{III} + 2\,e^- \longrightarrow 2\,HCo^{II}$$
$$2\,HCo^{II} \longrightarrow 2\,Co^{I} + H_2$$

Monometallic Pathway

$$HCo^{III} + e^- \longrightarrow HCo^{II}$$
$$HCo^{II} + HX \longrightarrow Co^{II} + X^- + H_2$$
$$Co^{II} + e^- \longrightarrow Co^{I}$$

different combinations of HCo^{III}, HCo^{II}, and HCo^{I} can participate in bimetallic and monometallic H−Co bond cleavage. In the present case, $[HCo^{III}(L2)(CH_3CN)]^{2+}$ and $[HCo^{III}(L3)(CH_3CN)]^{2+}$ are stable in acetonitrile solution, which eliminates the possibility of either a bimetallic pathway involving two HCo^{III} or a monometallic reaction of HCo^{III} with a trace protic impurity.

The monometallic and bimetallic pathways both produce Co^{I} at the electrode and may be differentiated by examining the voltammetry as a function of HCo^{III} concentration. The ratio i_{pa}'/i_{pc} provides a qualitative comparison of the amount of Co^{I} formed (i_{pa}') relative to the total concentration of cobalt species (i_{pc}), that is, the initial HCo^{III} concentration, and i_{pa}'/i_{pc} will increase with $[HCo^{III}]_o$ *only* if bimetallic routes are operative. As shown in Figure 3, i_{pa}'/i_{pc} actually decreases with

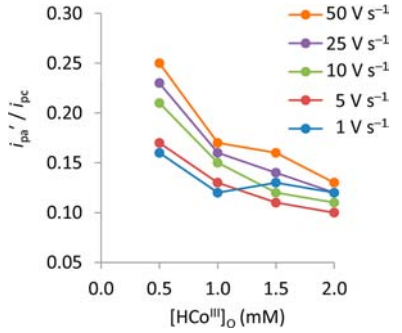

Figure 3. Plot of i_{pa}'/i_{pc} vs initial concentration of $[HCo^{III}(L2)(CH_3CN)]^{2+}$, where i_{pa}' is i_{pa} for the $[Co^{I}(L2)(CH_3CN)]^{+}$ oxidation. Conditions: 0.2 M NBu_4PF_6 acetonitrile solution, glassy carbon working electrode, 23 ± 2 °C.

increasing $[HCo^{III}]_o$ from 0.5 to 2.0 mM at $\upsilon \geq 1$ V s^{-1}, indicating that more Co^{I} is formed at lower initial concentrations of cobalt. This supports a monometallic mechanism in which HCo^{II}, HCo^{I}, or both lose H^- to a protic solvent impurity. The likely protic impurity is water, which can serve as a proton source to produce 1 equiv of H_2 per Co (e.g., Scheme 2, monometallic pathway). Acetonitrile dried as

dx.doi.org/10.1021/ic401232g | Inorg. Chem. 2013, 52, 9975−9988

Table 2. Optimized Simulation Parameters for Cyclic Voltammograms of $[HCo^{III}(L2)(CH_3CN)]^{2+}$[a]

Electron Transfer Reactions and Parameters[b]			
redox couple	E° (V vs $Cp_2Fe^{+/0}$)		k° (cm s^{-1})
$[HCo^{III/II}(L2)(CH_3CN)]^{2+/+}$	−1.5614(3)		0.025[c]
$[HCo^{II/I}(L2)]^{+/0}$	−1.4742(5)		0.28(2)
$[Co^{II/I}(L2)(CH_3CN)]^{2+/+}$	−0.82		0.1[d]
Chemical Reactions and Parameters			
reaction	K_{eq} (M)	k_{fwd} (s^{-1})	k_{rev}[e] (M^{-1} s^{-1})
$[HCo^{II}(L2)(CH_3CN)]^+ \rightleftharpoons [HCo^{II}(L2)]^+ + CH_3CN$	32(2)	1030(20)	32
$[HCo^{II}(L2)(CH_3CN)]^+ \rightarrow [Co^{II}(L2)(CH_3CN)]^{2+} + H^-$		128(2)	

[a]Uncertainties are given at the 2σ (95.4%) confidence level and are generated in the least-squares refinement. [b]Butler−Volmer transfer coefficient (α) was fixed at 0.5 for all electron transfer reactions. [c]Determined by manual iteration as described in the Experimental Section. [d]Determined by voltammogram simulation of isolated $[Co^{II}(L2)(CH_3CN)]^{2+}$. [e]$k_{rev} = k_{fwd}/K_{eq}$.

described in the Experimental Section typically contains 10−15 ppm water as determined by Karl Fischer titration (10 ppm water by mass = 0.4 mM water in acetonitrile). Deliberate addition of excess water (140 mM) to an acetonitrile solution of $[HCo^{III}(L2)(CH_3CN)]^{2+}$ (2 mM) rendered its reduction completely irreversible at scan rates of 1 V s^{-1} or less (Figure S6, Supporting Information), though partial reversibility was observed at higher scan rates (Figure S7, Supporting Information).

Bulk electrolysis of $[HCo^{III}(L2)(CH_3CN)]^{2+}$ (2 mM) at a potential of −1.81 V vs $Cp_2Fe^{+/0}$ resulted in the passage of 1.1 e^- per cobalt, and voltammetry of the solution after electrolysis indicated quantitative conversion to $[Co^{I}(L2)(CH_3CN)]^+$. These results indicate a net loss of $H^\bullet$ following reduction and a bimetallic mechanism for H_2 formation under these conditions. The slight excess of 0.1 electrons observed in the bulk electrolysis suggests that HCo^{II} or HCo^{I} may consume the trace water impurity in a monometallic pathway prior to or concurrent with bimetallic H_2 formation. A bulk electrolysis experiment with $[HCo^{III}]$ = 2.0 mM and $[H_2O]$ = 0.4 mM would afford 1.2 electrons per Co if the water were completely consumed in a monometallic reaction, in agreement with the result obtained within experimental error (see Supporting Information).

Two differences exist between the reactivity observed in the bulk electrolysis and cyclic voltammetry experiments. First, the extent of monometallic H−Co bond cleavage is limited by the water concentration in a bulk electrolysis experiment, whereas water can be recruited by diffusion from the bulk solution in a cyclic voltammetry experiment. Second, and perhaps more importantly, bimetallic H−Co bond cleavage is observed in the bulk electrolysis experiment, but not in the cyclic voltammetry experiments. This difference in apparent reactivity indicates that bimetallic H_2 formation pathways are prevalent on the time scale of an electrolysis experiment (ca. 20 min), but occur to a smaller extent on the time scale of a cyclic voltammetry experiment (≤1 s when $\upsilon \geq 1$ V s^{-1}).

Modeling of Voltammograms. The above analysis provides a qualitative description of the reactions that occur following reduction of $[HCo^{III}(L2)(CH_3CN)]^{2+}$. Digital simulations of the cyclic voltammograms were performed to examine the relative rates of mono- and bimetallic H−Co bond cleavage reactions, acetonitrile binding and dissociation, and the influence of electron transfer kinetics. Each of these reactions is relevant to electrocatalytic proton reduction. Experimental voltammograms of $[HCo^{III}(L2)(CH_3CN)]^{2+}$ were recorded at five scan rates ranging from 1 to 50 V s^{-1}, and analyte concentrations of 1.0, 1.5, and 2.0 mM were employed in the refinements of the digital simulations.

One conclusion drawn above is that reactions between two HCo complexes to form H_2 with net loss of $H^\bullet$ from each, while relevant in bulk electrolysis, are slow on the cyclic voltammetry time scale. Candidate reactants for a bimetallic pathway include $[HCo^{III}(L2)(CH_3CN)]^{2+}$, $[HCo^{II}(L2)(CH_3CN)]^+$, $[HCo^{II}(L2)]^+$, and $HCo^{I}(L2)$, and several combinations of these are reasonable (see the Supporting Information). The second-order rate constants, which will be independent of analyte concentration, were estimated by refinement against only the 1.0 mM data, and separately against only the 2.0 mM data, to assess the validity of the different bimetallic models. The estimated rate constants were consistently larger by a factor of 1.7 to 12.7 when the 1.0 mM data set was used (see the Supporting Information for tabulation of simulation parameters). This supports our conclusion that these bimetallic reactions, while favorable thermodynamically, do not contribute significantly to the observed voltammetric responses.

The monometallic routes were modeled as pseudo-first-order reactions; the concentration of the protic impurity is unknown but is continually replenished at the electrode by diffusion from the bulk solution. Acetonitrile solutions of $[HCo^{III}(L2)(CH_3CN)]^{2+}$ are stable prior to reduction, so the candidate hydride donors are $[HCo^{II}(L2)(CH_3CN)]^+$, $[HCo^{II}(L2)]^+$, and $HCo^{I}(L2)$. Monometallic routes for formation of H_2 leading to $[Co^{I}(L2)(CH_3CN)]^+$ were considered for each; however, only the $[HCo^{II}(L2)(CH_3CN)]^+$ model afforded both a first-order rate constant that was independent of cobalt concentration and an increased i_{pa}' for oxidation of $[Co^{I}(L2)(CH_3CN)]^+$ at all scan rates. An unconstrained simultaneous refinement on all parameters of the monometallic $[HCo^{II}(L2)(CH_3CN)]^+$ model was performed against all of the experimental data sets. Parameter estimates obtained from this refinement are given in Table 2, and selected simulated voltammograms are shown in Figure 4. The uncertainties provided in Table 2 (and in Tables S3−S14, Supporting Information) are given at the 2σ (95.4%) confidence level and are generated in the least-squares refinement. These error estimates indicate only how well the experimental data is fit by the chosen model and do not reflect the precision of the cyclic voltammetry technique, systematic errors in the experimental data, or the validity of the chosen model. Therefore we assume a larger uncertainty in the real values.

While the monometallic $[HCo^{II}(L2)(CH_3CN)]^+$ model provided the best fit to the experimental data, this model is not necessarily a unique solution. The reaction of water with

dx.doi.org/10.1021/ic401232g | Inorg. Chem. 2013, 52, 9975−9988

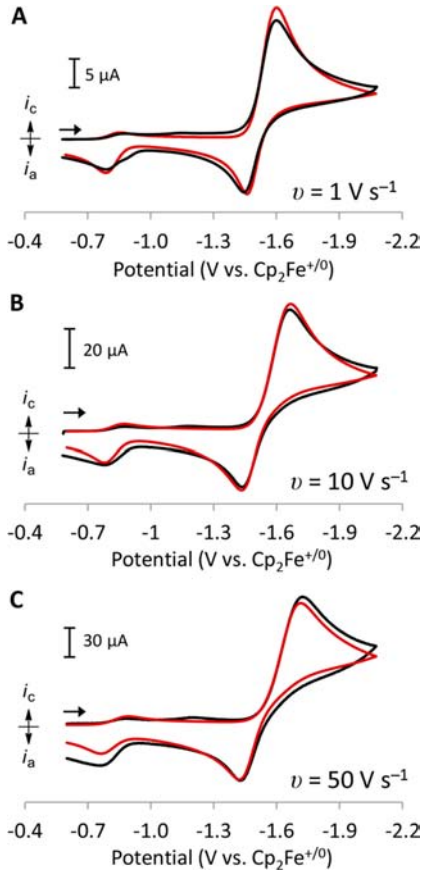

Figure 4. Experimental (black line) and simulated (red line) voltammograms for reduction of $[HCo^{III}(L2)(CH_3CN)]^{2+}$ (2 mM) at (A) υ = 1 V s^{-1}, (B) υ = 10 V s^{-1}, and (C) υ = 50 V s^{-1}. Simulations use the parameters listed in Table 2.

$HCo^{I}(L2)$ is likely more favorable than reaction with $[HCo^{II}(L2)(CH_3CN)]^{+}$, in accord with the experimental hydride donor abilities of $[HCo^{II}(dppe)_2]^{+}$ and $HCo^{I}(dppe)_2$.[48] Therefore a model was considered in which both $[HCo^{II}(L2)(CH_3CN)]^{+}$ and $HCo^{I}(L2)$ could participate in monometallic H−Co bond cleavage. However, refinement on this model afforded a rate constant for monometallic H−Co bond cleavage of $HCo^{I}(L2)$ that was 11 orders of magnitude smaller than that obtained for $[HCo^{II}(L2)(CH_3CN)]^{+}$. This result is inconsistent with the reactivity predicted from consideration of the HCo^{II} and HCo^{I} hydride donor abilities. We attribute this result to a limitation of the least-squares refinement procedure to handle a model containing two H−Co bond cleavage steps, and we believe that both $[HCo^{II}(L2)(CH_3CN)]^{+}$ and $HCo^{I}(L2)$ react with water during the course of recording a cyclic voltammogram.

As mentioned above, a voltammogram collected at υ = 50 V s^{-1} displayed a shoulder at −1.53 V on the second cathodic sweep when the potential was cycled repeatedly about the $[HCo^{III}(L2)(CH_3CN)]^{2+}$ reduction (Figure 2c). This data motivated inclusion of explicit acetonitrile dissociation and binding steps, and these were found to be necessary for satisfactory modeling of the experimental voltammograms. Mono- and bimetallic models not containing a reversible acetonitrile dissociation step predicted a severely diminished current for i_{pa}, i_{pa}', or both. As seen in Table 2, dissociation of acetonitrile from $[HCo^{II}(L2)(CH_3CN)]^{+}$ (k = 1030 s^{-1}) appears to be somewhat faster than acetonitrile coordination to $[HCo^{II}(L2)]^{+}$ (k = 576 s^{-1} in 18 M acetonitrile solvent). A simulation of the cyclic voltammogram cycling experiment (Figure 2c) using the refinement parameters shown in Table 2 did not display the expected shoulder at −1.53 V (Figure S8, Supporting Information). This indicates that the estimated lifetime of $[HCo^{II}(L2)]^{+}$ is too short, and the optimized rate constant for acetonitrile coordination is too large. Manually decreasing this rate constant from k = 576 to 247 s^{-1} affords simulated voltammograms showing this shoulder feature (Figure S9, Supporting Information). The difference in these barrier heights is 0.5 kcal mol^{-1}, which suggests that the optimized simulation parameters are reasonably accurate.

The simulations presented above reveal that the value of E_{pc} is predominantly a function of the rates of acetonitrile dissociation and electron transfer relative to the scan rate. At low scan rates, acetonitrile dissociation and electron transfer are both fast relative to the potential sweep, and the cathodic wave corresponds to the two-electron reduction of $[HCo^{III}(L2)(CH_3CN)]^{2+}$ to $HCo^{I}(L2)$. In this case E_{pc} (−1.57 V at υ = 0.1 V/s) approaches within −20 mV of the formal potential for the reduction of $[HCo^{III}(L2)(CH_3CN)]^{2+}$ to $[HCo^{II}(L2)]^{+}$, calculated at E^0_S = −1.55 V (eqs 4−6; subscript S indicates the reduction is coupled to dissociation of a solvent ligand). As the scan rate is increased, acetonitrile dissociation and electron transfer become slow relative to the potential sweep and E_{pc} shifts negative of the reversible $[HCo^{III/II}(L2)(CH_3CN)]^{2+/+}$ couple at −1.56 V.

Analysis of the cyclic voltammograms of $[HCo^{III}(L2)(CH_3CN)]^{2+}$ reveal that at a scan rate of 0.1 V s^{-1}, the experimentally measured values of E_{pc} (−1.57 V) and E_{pa} (−1.46 V) are very close to the formal potentials of the $[HCo^{III}(L2)(CH_3CN)]^{2+}/[HCo^{II}(L2)]^{+}$ (−1.55 V) and $[HCo^{II/I}(L2)]^{+/0}$ (−1.47 V) redox couples obtained from digital simulations. By applying this correlation to a cyclic voltammogram of $[HCo^{III}(L3)(CH_3CN)]^{2+}$ recorded at 0.1 V s^{-1}, one can estimate potentials of −1.29 and −1.21 V for the $[HCo^{III}(L3)(CH_3CN)]^{2+}/[HCo^{II}(L3)]^{+}$ and $[HCo^{II/I}(L3)]^{+/0}$ couples, respectively. This estimate of the $[HCo^{III}(L3)(CH_3CN)]^{2+}/[HCo^{II}(L3)]^{+}$ couple assumes that the equilibrium constant for acetonitrile dissociation from $[HCo^{II}(L3)(CH_3CN)]^{+}$ is similar to the equilibrium constant of 32 M that was determined (eq 5) for $[HCo^{II}(L2)(CH_3CN)]^{+}$.

DISCUSSION

Cobalt electrocatalysts for H_2 production typically display a catalytic current enhancement at the potential of the $Co^{II/I}$ couple, at the potential of the $Co^{I/0}$ couple, or at a potential between these two couples.[4] Comparison of the reduction potentials of possible catalytic intermediates to the observed catalytic wave can provide information about the mechanism, and mechanistic studies often focus on pathways for formation

$$[HCo^{III}(L2)(CH_3CN)]^{2+} + e^- \rightarrow [HCo^{II}(L2)(CH_3CN)]^{+} \quad \Delta G^\circ = -23.06 \times E^\circ(HCo^{III/II}) = 36.0 \text{ kcal/mol} \quad (4)$$

$$[HCo^{II}(L2)(CH_3CN)]^{+} \rightarrow [HCo^{II}(L2)]^{+} + CH_3CN \quad \Delta G^\circ = -1.364 \times \log(K_{eq}) = -0.3 \text{ kcal/mol} \quad (5)$$

$$[HCo^{III}(L2)(CH_3CN)]^{2+} + e^- \rightarrow [HCo^{II}(L2)]^{+} + CH_3CN \quad E^\circ_S(HCo^{III/II}) = -\Delta G^\circ \div 23.06 = -1.55 \text{ V} \quad (6)$$

dx.doi.org/10.1021/ic401232g | Inorg. Chem. 2013, 52, 9975−9988

of HCo^{III} and HCo^{II}.[7,32,33] Knowledge of the chemical reactivity of hydride intermediates on the voltammetry time scale in the absence of added protons can provide information about the mechanism(s) of electrocatalytic H_2 formation. In cases where reduction of a cobalt hydride intermediate determines the electrocatalytic overpotential, examination of the structural factors that control their redox properties can aid the development of more energy-efficient electrocatalysts.

This study was designed to investigate the chemical and electrochemical reactivity of possible cobalt hydride intermediates in electrocatalytic hydrogen production by cobalt complexes containing pendant amines. The previously reported electrocatalysts, $[Co^{II}(P^{R}_{2}N^{R'}_{2})(CH_3CN)_3]^{2+}$, underwent ligand exchange reactions that complicated mechanistic investigations.[39−41] New tetradentate phosphine ligands containing pendant amines (L2 and L3) were found to greatly increase the stability of these intermediates. The Co^{II} and Co^{I} complexes, $[Co^{II}(L2/L3)(CH_3CN)]^{2+}$ and $[Co^{I}(L2/L3)(CH_3CN)]^{+}$, are similar to previously studied $[Co^{II}(diphosphine)_2(CH_3CN)]^{2+}$ and $[Co^{I}(diphosphine)_2(CH_3CN)]^{+}$ complexes.[48,49] Additionally, the HCo^{III} complexes $[HCo^{III}(L2/L3)(CH_3CN)]^{2+}$ are structurally analogous to $[HCo^{III}(dppe)_2(CH_3CN)]^{2+}$,[48] and these hydride complexes all display similar spectroscopic features and stability toward H_2 elimination. Importantly, $[Co^{II}(L2)(CH_3CN)]^{2+}$ and $[Co^{II}(L3)(CH_3CN)]^{2+}$ are also electrocatalysts for H_2 production, and their catalytic activity will be reported separately.

The voltammetry of $[HCo^{III}(L2)(CH_3CN)]^{2+}$ reflects a composite of several processes: formation of HCo^{I} through an $E_rC_rE_r$ pathway (Scheme 1), monometallic reaction of HCo^{II} (and possibly HCo^{I}) with a trace solvent impurity, and the kinetics of the HCo^{III} reduction step. While simulation models for various bimetallic H−Co bond cleavage reactions could approximate individual experimental voltammograms reasonably well, significant discrepancies were observed for the bimetallic rate constants obtained from refinements of voltammograms recorded at different analyte concentrations. On the other hand, refinement of models based on monometallic H−Co bond cleavage resulted in nearly identical rate constants at different analyte concentrations. These observations strongly suggest that monometallic reaction of the reduced cobalt hydride species is kinetically relevant on the voltammetry time scale, while bimetallic reactions are not kinetically important for cyclic voltammetry. In contrast, Koelle and Ohst reported cyclic voltammetry studies in which reduction of $HCo^{III}(Cp)(dppv)$ (dppv = $Ph_2PCH{=}CHPPh_2$) in the absence of acid produces H_2 through a bimetallic reaction mechanism, with an estimated lower limit of 5000 M^{-1} s^{-1} for the second-order rate constant.[53] Recent results from Kaim and co-workers show that electrochemical oxidation of $HCo^{I}(CO)_2(dippf)_2$ (dippf = 1,1′-bis(diisopropylphosphino)-ferrocene) results in H_2 formation, which is proposed to occur through a bimetallic pathway on the voltammetry time scale.[54]

However, bimetallic pathways are kinetically relevant for $[HCo^{III}(L2)(CH_3CN)]^{2+}$ on the time scale of an electrolysis experiment, ca. 25 min, as evidenced by the passage of 1.1 e^- per $[Co^{I}(L2)(CH_3CN)]^{+}$ generated. This is in stark contrast to $[HCo^{II}(dppe)_2]^{+}$, which is stable in solution for greater than 18 h despite a favorable driving force for bimetallic H_2 elimination (ΔG = −3.6 kcal mol^{-1}).[48] One explanation for this difference in reactivity is that the pendant amine of $[HCo^{III}(L2)-(CH_3CN)]^{2+}$ can facilitate an intermolecular proton transfer to $[HCo^{II}(L2)(CH_3CN)]^{+}$ or $HCo^{I}(L2)$, which will result in H_2 formation and the passage of 1 e^- per $[Co^{I}(L2)(CH_3CN)]^{+}$ generated. This is relevant in the context of experiments performed in the absence of acid but not necessarily for electrocatalysis experiments conducted in the presence of substantial amounts of acid.

Relationships between Structure and Redox Potential. The complexes $[Co^{II}(L2)(CH_3CN)]^{2+}$ and $[Co^{II}(L3)-(CH_3CN)]^{2+}$ both display a $Co^{II/I}$ redox couple at −0.82 V. This redox potential is intermediate between the $E_{1/2}$ values of −0.70 and −0.95 V observed for the cobalt complexes $[Co^{II}(dppe)_2(CH_3CN)]^{2+}$ and $[Co^{II}(dedpe)_2(CH_3CN)]^{2+}$ (dedpe = $Et_2PCH_2CH_2PPh_2$).[48,49] The qualitative ordering of these redox potentials follows the electron donor ability of the phosphine ligands, which is expected since the reduction of a square pyramidal Co^{II} complex (d^7) to a square pyramidal Co^{I} complex (d^8) does not involve a significant structural rearrangement of the phosphine coordination geometry.

In contrast, the $Co^{I/0}$ couple is a d^8 to d^9 reduction process that is isoelectronic to the $Ni^{II/I}$ couple, and the ability of the phosphine ligands to adopt a tetrahedral geometry strongly affects this redox couple. Previous studies on $[M^{II}(diphosphine)_2]^{2+}$ (M = Ni, Pd, Pt) complexes demonstrated that the $M^{II/I}$ redox couples are affected significantly by the diphosphine bite angle.[55−58] Computational investigations revealed that this phenomenon is a result of structural distortion from a square planar to a tetrahedral geometry as the ligand bite angle increases.[55] This tetrahedral distortion lowers the energy of the metal LUMO, which results in a more positive reduction potential. The complex $[Co^{I}(L2)-(CH_3CN)]^{+}$ is constrained to a square planar arrangement of the L2 ligand, and it has a very negative $Co^{I/0}$ couple of E_{pc} = −2.52 V. With the larger bite angle of the L3 ligand, the $Co^{I/0}$ couple of $[Co^{I}(L3)(CH_3CN)]^{+}$ is shifted positive to E_{pc} = −2.20 V. However, the $Co^{I/0}$ couple of $[Co^{I}(L3)(CH_3CN)]^{+}$ is still more negative than the $Co^{I/0}$ couple of $[Co^{I}(dedpe)_2(CH_3CN)]^{+}$ (−1.91 V), which is free to adopt a tetrahedral geometry upon reduction to Co^{0}.[49]

The $HCo^{III/II}$ redox potentials, which are influenced by acetonitrile dissociation, become more negative in the order $[HCo^{III}(dppe)_2(CH_3CN)]^{2+}$ (−0.83 V) > $[HCo^{III}(L3)-(CH_3CN)]^{2+}$ (−1.29 V) > $[HCo^{III}(L2)(CH_3CN)]^{2+}$ (−1.55 V). This sequence follows the order of the analogous $Co^{I/0}$ couples and suggests that the five-coordinate HCo^{II} reduction products are also stabilized by a dihedral twist of the phosphine ligands from a planar geometry. While no $[HCo^{II}(diphosphine)_2]^{+}$ complexes were found in a search of the Cambridge Crystallographic Database, many $HCo^{I}(diphosphine)_2$ and related complexes have been crystallographically characterized. In particular, $HCo^{I}(dppe)_2$, $HCo^{I}(dedpe)_2$, and $HCo^{I}(dmpe)_2$ have P−Co−P angles of approximately 90°,[48,49] which is similar to that of the tetradentate L2 and L3 ligands. These HCo^{I} complexes are best described as square pyramids with the hydride ligand occupying a basal position, and similar geometries are expected for the HCo^{II} analogues of these species. Therefore the reduction from $[HCo^{III}(dppe)_2(CH_3CN)]^{2+}$ to $[HCo^{II}(dppe)_2]^{+}$ induces a dihedral twist similar to the reduction of Co^{I} to Co^{0}. However, it is difficult for the rigid tetradentate phosphine ligands of $[HCo^{II}(L2)]^{+}$ and $[HCo^{II}(L3)]^{+}$ to undergo a dihedral twist, so the hydride ligands of these complexes will possess more *axial* character than $[HCo^{II}(dppe)_2]^{+}$. This geometric constraint leads to a destabilization of the HCo^{II} species and results in sequentially

dx.doi.org/10.1021/ic401232g | Inorg. Chem. 2013, 52, 9975−9988

more negative $HCo^{III/II}$ couples for $[HCo^{III}(L3)(CH_3CN)]^{2+}$ and $[HCo^{III}(L2)(CH_3CN)]^{2+}$. A similar trend is observed for the $HCo^{II/I}$ redox potentials, where the $[HCo^{II/I}(L2)]^{+/0}$ couple (−1.47 V) is more negative than the $[HCo^{II/I}(L3)]^{+/0}$ couple (−1.21 V).

Relevance to Cobalt H_2 Production Electrocatalysts. The above analysis of the influence of molecular geometry on various cobalt redox potentials is useful for predicting trends of cobalt tetraphosphine systems. We anticipate that these concepts can be extended to other cobalt systems, which would be valuable toward understanding and predicting the redox chemistry of cobalt hydride species that are intermediates of electrocatalytic H_2 production. However, factors such as molecular charge can also influence the redox potentials of HCo^{III} species, and it is difficult to identify geometric trends across a range of different ligand types given the limited number of HCo^{III} complexes that have been characterized by cyclic voltammetry.

The possibility of a HCo^{I} intermediate is not commonly considered in mechanistic investigations of electrocatalytic H_2 production by molecular cobalt complexes. The present work demonstrates that a HCo^{I} complex, $HCo^{I}(L2)$, is formed at the same potential as the HCo^{II} complex, $[HCo^{II}(L2)]^{+}$, and prior voltammetry studies[48] demonstrated overlapping reduction waves for the $HCo^{III/II}$ and $HCo^{II/I}$ couples of $[HCo^{III}(dppe)_2(CH_3CN)]^{2+}$. These HCo^{I} species are formed at potentials of relevance to electrocatalytic H_2 production, that is, positive of the $Co^{I/0}$ couple; therefore, it is of interest to consider whether similar behavior can be generally expected of other cobalt systems. For a given cobalt system, the $Co^{I/0}$ and $HCo^{II/I}$ redox couples are thermodynamically related to the solution homolytic bond dissociation free energies ($\Delta G^{\circ}_{H\bullet}$) of both the HCo^{II} and HCo^{I} species as illustrated in Scheme 3.

Scheme 3. Thermochemical Relationship Between Reduction Potential and Cobalt−Hydride Solution Homolytic Bond Dissociation Free Energy

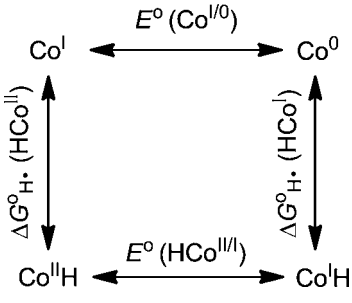

This relationship can be expressed mathematically as shown in eq 7 using known thermochemical cycles[48,59−62] and will be true even in cases where the formal $Co^{I/0}$ or $HCo^{II/I}$ reductions are ligand-centered.[6,18] Equation 7 reveals that the potential of the $HCo^{II/I}$ couple can be estimated to be either positive or negative of the $Co^{I/0}$ couple if the relative values of $\Delta G^{\circ}_{H\bullet}$ for HCo^{II} and HCo^{I} are known.

$$E^{\circ}(HCo^{II/I}) = E^{\circ}(Co^{I/0}) + \frac{\Delta G^{\circ}_{H\bullet}(HCo^{I}) - \Delta G^{\circ}_{H\bullet}(HCo^{II})}{23.06} \quad (7)$$

If the potential of the $HCo^{II/I}$ couple is *negative* of the $Co^{I/0}$ couple in a given catalytic system, then a HCo^{I} intermediate can be excluded from mechanistic consideration. This possibility requires the open-shell (d^7) HCo^{II} species to be more stable toward homolysis, that is, larger $\Delta G^{\circ}_{H\bullet}$, than the closed-shell (d^8) HCo^{I} species as illustrated by eq 7. However, the opposite trend in metal−hydride bond stability is typically observed: closed-shell metal hydrides have larger $\Delta G^{\circ}_{H\bullet}$ values than their open-shell counterparts. This trend has been observed experimentally for hydride complexes of chromium,[63] molybdenum,[64] tungsten,[64,65] iron,[66] cobalt,[48] rhodium,[67] and platinum,[68] and has been predicted for nickel using DFT computations.[69] Additionally, the S−H bonds of the closed-shell complexes $Cp^*_2Mo_2S_3(SH)$, $Cp^*_2Mo_2S_2(SH)_2$, and $Cp^*_2Mo_2S_2(SMe)(SH)$ all have larger $\Delta G^{\circ}_{H\bullet}$ values than their open-shell counterparts obtained upon either oxidation or reduction by one electron.[70] An example of the reverse trend has been reported: the W−H bond of open-shell $[Cp^*(dppe)WH_3]^{+}$ has a larger $\Delta G^{\circ}_{H\bullet}$ value than closed-shell $Cp^*(dppe)WH_3$ as determined from infrared spectroscopy and DFT computations.[71,72] It is reasonable to expect that most cobalt systems will follow the typically observed trend, and the H−Co bond of an open-shell HCo^{II} complex will have a smaller $\Delta G^{\circ}_{H\bullet}$ value than its closed-shell HCo^{I} counterpart. As a result, a HCo^{II} intermediate will likely be reduced to HCo^{I} at potentials positive of the $Co^{I/0}$ couple for most cobalt H_2 production electrocatalysts according to the relationship described by eq 7. Consequently a HCo^{I} species should be considered as a potential catalytic intermediate in mechanistic investigations.

Consideration of a HCo^{I} intermediate increases the mechanistic complexity of electrocatalytic H_2 production using molecular cobalt complexes. Depending on the experimental conditions, cobalt hydride intermediates can be formed in three metal oxidation states by a variety of protonation and reduction sequences. Additionally, reduction of HCo^{II} to HCo^{I} may require prior ligand dissociation from HCo^{II}, and the kinetics of this step may vary widely among different catalyst platforms. These steps directly affect the catalytic overpotential, which is determined by the strength of the acid and by the potential of electrocatalysis. Additionally, a HCo^{I} intermediate is likely to be a stronger hydride donor than a HCo^{II} intermediate,[48,49] which is potentially beneficial for electrocatalytic proton reduction. However, as recently indicated by Gray and co-workers,[7] a HCo^{I} intermediate may be detrimental to catalysis if it can be protonated to form a stable $(H)_2Co^{III}$ complex[48,49,73,74] under electrocatalytic conditions. Knowledge of the thermodynamic properties of the possible intermediates is expected to facilitate catalyst development. In a subsequent paper, we will describe the electrocatalytic formation of H_2 by $[Co^{II}(L2)(CH_3CN)]^{2+}$ and $[Co^{II}(L3)(CH_3CN)]^{2+}$ and investigate the role of various intermediates in the catalytic cycle.

SUMMARY AND CONCLUSIONS

By employing a tetradentate phosphine ligand, we isolated and characterized the HCo^{III} complexes $[HCo^{III}(L2)(CH_3CN)]^{2+}$ and $[HCo^{III}(L3)(CH_3CN)]^{2+}$, which each possess pendant amines. Electrochemical reduction of these complexes activates the H−Co bond toward cleavage. Analysis of the voltammograms suggests a monometallic reaction between the reduced cobalt hydride and a solvent impurity, while bulk electrolysis experiments suggest a bimetallic reaction between two cobalt hydride species. Digital simulations confirmed that the

dx.doi.org/10.1021/ic401232g | Inorg. Chem. 2013, 52, 9975−9988

monometallic pathway is dominant on the voltammetry time scale. Additionally, digital simulations revealed the presence of an $E_rC_rE_r$ reduction mechanism for $[HCo^{III}(L2)(CH_3CN)]^{2+}$, which ultimately forms $HCo^{I}(L2)$, a HCo^{I} complex, upon dissociation of an acetonitrile ligand from $[HCo^{II}(L2)(CH_3CN)]^{+}$, a HCo^{II} complex. These results are significant because HCo^{III} and HCo^{II} complexes are believed to be important intermediates in electrocatalyic H_2 production, yet they can rarely be analyzed due to their high reactivity. Furthermore, these results indicate that HCo^{I} complexes, while seldom considered as catalytic intermediates, may also be important intermediates in electrocatalytic and photocatalytic H_2 production.

EXPERIMENTAL SECTION

Methods and Materials. All manipulations were carried out under N_2 using standard vacuum line, Schlenk, and inert-atmosphere glovebox techniques. THF (Alfa-Aesar, anhydrous, nonstabilized), acetonitrile (Alfa-Aesar, anhydrous, amine-free), dichloromethane (Fisher), hexane (Honeywell), and diethyl ether (Burdick & Johnson) were purified by sparging with N_2 and passage through neutral alumina, and ethanol (Pharmco-Aaper absolute anhydrous) was purified by sparging with N_2 and passage through calcium sulfate, using an Innovative Technology, Inc., Pure Solv solvent purification system. Water was dispensed from a Millipore Milli-Q purifier and sparged with nitrogen. Acetonitrile-d_3 (Cambridge Isotope Laboratories) was vacuum-distilled from P_2O_5. Chloroform-*d* (Cambridge Isotope Laboratories) was degassed by three freeze−pump−thaw cycles and dried over 4 Å molecular sieves. Tetrabutylammonium hexafluorophosphate (Fluka, ≥99%) was used as received. Tetraethylammonium tetrafluoroborate (Alfa-Aesar) was recrystallized twice from CH_3CN/Et_2O and dried under vacuum at room temperature. *p*-Bromoanilinium tetrafluoroborate was prepared by reaction of the substituted aniline with 1.5 equiv of $HBF_4{\cdot}Et_2O$ followed by recrystallization from CH_3CN/Et_2O. Ferrocene (Aldrich) was sublimed under vacuum before use. Diphenylphosphine (Strem, 99%), diethyl vinylphosphonate (Acros, 97%), diethyl allylphosphonate (Acros, 97%), 2,2′-azobis(2-methylpropionitrile) (AIBN, Aldrich, 97%), lithium aluminum hydride (Aldrich, 95%), chlorotrimethylsilane (Aldrich, 99%), paraformaldehyde (Aldrich, 95%), aniline (Aldrich, 99%), and *p*-bromoaniline (Aldrich, 97%) were used as received. $[Co(CH_3CN)_6](BF_4)_2$[75,76] was prepared according to literature procedures. $Ph_2PCH_2CH_2PH_2$[42] and $Ph_2PCH_2CH_2CH_2PH_2$[43] were prepared using modified literature procedures, as detailed in the Supporting Information.

Instrumentation. ^1H and ^{31}P NMR spectra were recorded on a Varian Inova spectrometer (500 MHz for ^1H) at 25 °C. All ^1H chemical shifts have been internally calibrated to the monoprotio impurity of the deuterated solvent. The ^{31}P NMR spectra were referenced to external phosphoric acid at 0 ppm. NMR simulations were performed using the line-fitting feature of MestReNova v6.0.4. Magnetic moments were determined by Evans method[77−79] in CD_3CN solution. Elemental analyses were performed by Atlantic Microlab, Inc.

Voltammetry measurements were performed using a CH Instruments 620D potentiostat equipped with a standard three-electrode cell. Experiments were performed in a glovebox at ambient temperature, 23 ± 2 °C, using a 4−5 mL conical glass vial fitted with a polysilicone cap having openings sized to closely accept each electrode. The working electrode (1 mm PEEK-encased glassy carbon, Cypress Systems EE040) was polished using diamond paste (Buehler, 0.25 μm) on a polishing pad wet with purified H_2O, then the electrode was rinsed with neat acetonitrile. A glassy carbon rod (Structure Probe, Inc.) was used as the counterelectrode, and a silver wire suspended in a solution of Bu_4NPF_6 (0.2 M) in acetonitrile and separated from the analyte solution by a Vycor frit (CH Instruments 112) was used as a pseudoreference electrode. Ferrocene was used as an internal standard, and all potentials are referenced to the ferrocenium/ferrocene couple at 0 V. Controlled potential electrolyses were performed using a CH Instruments 1100A power potentiostat.

Syntheses. *Bis(hydroxymethyl)(2-diphenylphosphinoethyl)-phosphine.* Diphenyl(2-phosphinoethyl)phosphine (3.04 g, 0.0123 mol), paraformaldehyde (3.63 g, 0.121 mol, 9.8 equiv), and CH_3CN (100 mL) were combined in a 250 mL Schlenk flask. The mixture was heated overnight in a 65 °C oil bath, then the mixture was filtered, and the filtrate was concentrated to dryness. The resulting oil was evacuated while heating at 100 °C for 3 h, which afforded bis(hydroxymethyl)(2-phosphinoethyl)phosphine (2.20 g) as a white solid. $^{31}P\{^1H\}$ NMR spectroscopy indicated the product was approximately 66% pure. Less product decomposition occurred by conducting the evacuation step at lower temperatures for longer periods of time. However, the product could not be obtained consistently in this manner on larger scales, presumably due to poor mass transport of CH_2O within the viscous product medium. ^1H NMR (500 MHz, $CDCl_3$): δ 7.47−7.42 (m, 4H, Ar*H*), 7.37−7.32 (m, 6H, Ar*H*), 4.32 (dd, 2H, $^2J_{HH}$ = 13.4 Hz, $^2J_{HP}$ = 10.0 Hz, $P(CH_AH_BOH)_2$), 4.12 (dd, 2H, $^2J_{HH}$ = 13.4 Hz, $^2J_{HP}$ = 6.7 Hz, $P(CH_AH_BOH)_2$), 2.62 (br s, 2H, O*H*), 2.23 (m, 2H, $P(CH_2)_2P$), 1.91 (m, 2H, $P(CH_2)_2P$). $^{31}P\{^1H\}$ NMR ($CDCl_3$): δ −12.74 (d, 1P, $^3J_{PP}$ = 31.4 Hz, PPh_2), −18.79 (d, 1P, $^3J_{PP}$ = 31.4 Hz, $P(CH_2OH)_2$).

Bis(hydroxymethyl)(2-diphenylphosphinopropyl)phosphine. This compound was prepared in a manner analogous to that described for diphenyl(2-phosphinoethyl)phosphine, using 5.44 g (0.0209 mol) of diphenyl(2-phosphinopropyl)phosphine and 6.30 g (0.210 mol, 10 equiv) of paraformaldehyde. The crude oil was evacuated while heating at 70 °C for 8 h, to afford the product as a white solid (6.33 g). $^{31}P\{^1H\}$ NMR spectroscopy indicated the product was approximately 87% pure. ^1H NMR (300 MHz, $CDCl_3$): δ 7.47−7.39 (m, 4H, Ar*H*), 7.38−7.30 (m, 6H, Ar*H*), 4.32 (m, 2H, $P(CH_AH_BOH)_2$), 4.07 (m, 2H, $P(CH_AH_BOH)_2$), 3.00−2.62 (br s, 2H, O*H*), 2.23 (m, 2H, $P(CH_2)_3P$), 1.97 (m, 2H, $P(CH_2)_3P$), 1.71 (m, 2H, $P(CH_2)_3P$). $^{31}P\{^1H\}$ NMR ($CDCl_3$): δ −16.75 (s, 1P, PPh_2), −23.68 (s, 1P, $P(CH_2OH)_2$).

L2. Crude bis(hydroxymethyl)(2-phosphinoethyl)phosphine (2.99 g) was dissolved in EtOH (60 mL) in a 100 mL Schlenk flask. Aniline (0.88 mL, 9.7 mmol) was added to the solution via syringe, then the flask was immersed overnight in a 65 °C oil bath, causing a white precipitate to form. After cooling to room temperature, the mixture was filtered, and the solid was rinsed with EtOH (20 mL) and Et_2O (2 × 20 mL) to afford L2 (1.69 g, 2.33 mmol, 48% based on aniline) as a white powder. ^1H NMR (500 MHz, $CDCl_3$): δ 7.47−7.41 (m, 8H, Ar*H*), 7.40−7.31 (m, 12H, Ar*H*), 7.19 (m, 4H, Ar*H*), 6.68 (m, 6H, Ar*H*), 4.14 (dd, 4H, $^2J_{HH}$ = 15.0 Hz, $^2J_{HP}$ = 13.6 Hz, $PCH_{eq}H_{ax}N$), 3.36 (dd, 4H, $^2J_{HH}$ = 15.0 Hz, $^2J_{HP}$ = 4.2 Hz, $PCH_{eq}H_{ax}N$), 2.29 (m, 4H, $P(CH_2)_2P$), 1.44 (m, 4H, $P(CH_2)_2P$). $^{31}P\{^1H\}$ NMR ($CDCl_3$): δ −11.90 (d, 2P, $^3J_{PP}$ = 24.8 Hz, PPh_2), −45.67 (br d, 2P, $^3J_{PP}$ = 24.8 Hz, P_2N_2). Anal. Calcd for $C_{44}H_{46}N_2P_4$: C, 72.72; H, 6.38; N, 3.85. Found: C, 72.65; H, 6.24; N, 3.85.

L3. Crude bis(hydroxymethyl)(2-phosphinopropyl)phosphine (6.33 g) was dissolved in CH_3CN (125 mL) inside of a 250 mL Schlenk flask. Aniline (1.80 mL, 19.8 mmol) was added to the solution via syringe; then the flask was immersed in a 65 °C oil bath for 15 h, leading to the formation of a white precipitate. After cooling to room temperature, the solvent was removed under vacuum, and the solid was washed with Et_2O (3 × 30 mL). The crude product was precipitated twice from CH_2Cl_2/Et_2O at −35 °C and rinsed with Et_2O (20 mL) to afford L3 (2.70 g, 3.58 mmol, 36% based on aniline) as a white powder. ^1H NMR (500 MHz, $CDCl_3$): δ 7.47−7.41 (m, 8H, Ar*H*), 7.37−7.28 (m, 12H, Ar*H*), 7.14 (dd, 4H, $^3J_{HH}$ = 8.6, 7.3 Hz, Ar*H*), 6.64 (t, 2H, $^3J_{HH}$ = 7.3 Hz, Ar*H*), 6.59 (d, 4H, $^3J_{HH}$ = 8.6 Hz, Ar*H*), 4.09 (dd, 4H, $^2J_{HH}$ = 15.0 Hz, $^2J_{HP}$ = 12.9 Hz, $PCH_{eq}H_{ax}N$), 3.39 (dd, 4H, $^2J_{HH}$ = 15.0 Hz, $^2J_{HP}$ = 3.9 Hz, $PCH_{eq}H_{ax}N$), 2.22 (m, 4H, $P(CH_2)_3P$), 1.75 (m, 4H, $P(CH_2)_3P$), 1.53 (m, 4H, $P(CH_2)_3P$). $^{31}P\{^1H\}$ NMR ($CDCl_3$): δ −16.67 (s, 2P, PPh_2), −50.88 (br s, 2P, P_2N_2). Anal. Calcd for $C_{44}H_{46}N_2P_4$: C, 73.20; H, 6.68; N, 3.71. Found: C, 73.29; H, 6.54; N, 3.63.

$[Co^{II}(L2)(CH_3CN)](BF_4)_2$. A solution of $[Co(CH_3CN)_6](BF_4)_2$ (0.692 g, 1.45 mmol) in CH_3CN (5 mL) was added to a suspension of L2 (1.049 g, 1.443 mmol) in CH_3CN (50 mL). The resulting dark

dx.doi.org/10.1021/ic401232g | Inorg. Chem. 2013, 52, 9975−9988

brown solution was stirred for 1 h, then the solvent was removed under vacuum. The resulting residue was stirred overnight in hexane (40 mL), then the mixture was filtered, and the light brown powder was dried under vacuum to afford $[Co^{II}(L2)(CH_3CN)](BF_4)_2$ (1.255 g, 1.255 mmol, 87%). ^{1}H NMR (500 MHz, CD_3CN): δ 8.68 (br s, $\Delta\nu_{1/2}$ = 63 Hz), 7.54 (br s, $\Delta\nu_{1/2}$ = 26 Hz), 6.92 (br s, $\Delta\nu_{1/2}$ = 89 Hz), 5.58 (br s, $\Delta\nu_{1/2}$ = 73 Hz). μ_{eff} = 2.30 μ_B. Anal. Calcd for $C_{46}H_{49}B_2CoF_8N_3P_4$: C, 55.23; H, 4.94; N, 4.20. Found: C, 54.54; H, 5.11; N, 4.36.

[Co^{II}(L3)(CH$_3$CN)](BF$_4$)$_2$. Over a time period of 1 h, 30 min, a solution of $[Co(CH_3CN)_6](BF_4)_2$ (0.301 g, 0.629 mmol) in CH_3CN (12 mL) was added to a suspension of L3 (0.478 g, 0.634 mmol) in CH_3CN (30 mL). The resulting orange-brown solution was stirred for 10 min, then the solvent was removed under vacuum. The resulting residue was triturated overnight in hexane (30 mL), then the mixture was filtered, and the orange-brown powder was dried under vacuum to afford $[Co^{II}(L3)(CH_3CN)](BF_4)_2$ (0.535 g, 0.520 mmol, 83%). ^{1}H NMR (500 MHz, CD_3CN): δ 8.68 (br s, $\Delta\nu_{1/2}$ = 65 Hz), 7.53 (br s, $\Delta\nu_{1/2}$ = 25 Hz), 6.56 (br s, $\Delta\nu_{1/2}$ = 111 Hz), 5.91 (br m). μ_{eff} = 2.20 μ_B. Anal. Calcd for $C_{48}H_{53}B_2CoF_8N_3P_4$: C, 56.06; H, 5.19; N, 4.09. Found: C, 55.22; H, 5.12; N, 4.34.

[Co^{I}(L2)(CH$_3$CN)]BF$_4$. Solid $[Co^{II}(L2)(CH_3CN)](BF_4)_2$ (0.244 g, 0.244 mmol) was added to a stirring suspension of KC_8 (0.033 g, 0.24 mmol) in CH_3CN (12 mL). The mixture was stirred for 45 min, then the solvent was removed. The residue was stirred with THF (10 mL) for 1 h, then the mixture was allowed to settle overnight. The mixture was filtered through Celite, and the Celite was rinsed with excess THF. The purple filtrate was concentrated to dryness, then the residue was dissolved in acetonitrile (2 mL) to afford an orange solution. Diethyl ether (20 mL) was added to the acetonitrile solution, causing an orange powder to precipitate. The mixture was cooled to −35 °C, then the powder was collected by filtration, washed with Et_2O (2 × 5 mL), and dried under vacuum to afford $[Co^{I}(L2)(CH_3CN)]BF_4{\cdot}(KBF_4)_{0.5}$ (103 mg, 0.105 mmol, 43%). The amount of KBF_4 present was determined by integration of the ^{1}H and ^{19}F NMR spectra relative to added $[NBu_4]PF_6$. ^{1}H NMR (500 MHz, CD_3CN): δ 7.32 (t, 4H, $^3J_{HH}$ = 7.7 Hz, ArH), 7.24 (t, 4H, $^3J_{HH}$ = 7.0 Hz, ArH), 7.10 (d, 4H, $^3J_{HH}$ = 8.0 Hz, ArH), 7.02 (m, 8H, ArH), 6.99−6.91 (m, 10H, ArH), 3.85 (br d, 4H, $^2J_{HH}$ = 13.1 Hz, PCH_2CN), 3.52 (d, 4H, $^2J_{HH}$ = 13.1 Hz, PCH_2N), 2.52 (m, 4H, $P(CH_2)_2P$), 2.19 (m, 4H, $P(CH_2)_2P$). ^{31}P{^{1}H} NMR (CD_3CN): δ 77.1 (br d, 2P, $^2J_{PP}$ = 70 Hz), 73.5 (br d, 2P, $^2J_{PP}$ = 70 Hz). Anal. Calcd for $C_{46}H_{49}B_{1.5}CoF_6K_{0.5}N_3P_4$: C, 56.58; H, 5.06; N, 4.30. Found: C, 56.80; H, 5.03; N, 4.08.

[Co^{I}(L3)(CH$_3$CN)](BF$_4$). A solution of $[Co^{II}(L3)(CH_3CN)](BF_4)_2$ (0.014 g, 0.014 mmol) in CD_3CN (ca. 1 mL) was added to solid KC_8 (3 mg, 0.02 mmol, ca. 1.4 equiv). The mixture was stirred for 1 h and filtered through a small plug of Celite, and the orange filtrate was analyzed by NMR spectroscopy. ^{1}H NMR (500 MHz, CD_3CN): δ 7.31 (t, 4H, $^3J_{HH}$ = 7.9 Hz, ArH), 7.20−7.12 (m, 12H, ArH), 7.06 (d, 4H, $^3J_{HH}$ = 8.2 Hz, ArH), 6.98−6.91 (m, 10H, ArH), 3.38 (s, 8H, PCH_2CN), 2.34 (m, 4H, $P(CH_2)_3P$), 2.04−1.95 (br m, 9H, $P(CH_2)_3P$ + CH_3CN). ^{31}P{^{1}H} NMR (CD_3CN): δ 20.1 (m, 2P), 11.2 (m, 2P).

[HCo^{III}(L2)(CH$_3$CN)](BF$_4$)$_2$. Solid KC_8 (0.052 g, 0.39 mmol, 1.6 equiv) was added to a stirring solution of $[Co^{II}(L2)(CH_3CN)](BF_4)_2$ (0.251 g, 0.250 mmol) in CH_3CN (12 mL). After being stirred for 2.5 h, the mixture was filtered through Celite, and solid *p*-bromoanilinium tetrafluoroborate (0.072 g, 0.28 mmol, 1.1 equiv) was added to the orange filtrate. The resulting yellow solution was stirred for 45 min, then the solvent was removed under vacuum. The residue was extracted with CH_2Cl_2 (2 × 5 mL) and filtered through Celite, and the filtrate was concentrated under vacuum. The residue was triturated overnight in Et_2O (10 mL), then the mixture was filtered, and the resulting yellow powder was rinsed with Et_2O (2 × 5 mL) and dried under vacuum to afford $[HCo^{III}(L2)(CH_3CN)](BF_4)_2$ (0.174 g, 0.174 mmol, 70%). The isolated product contained trace quantities of $[Co^{II}(L2)(CH_3CN)](BF_4)_2$ as determined by ^{1}H NMR spectroscopy. ^{1}H NMR (500 MHz, CD_3CN): δ 7.59 (t, 2H, $^3J_{HH}$ = 7.4 Hz, ArH), 7.49−7.37 (m, 6H), 7.35 (t, 4H, $^3J_{HH}$ = 7.2 Hz, ArH), 7.27 (d, 2H, $^3J_{HH}$ = 7.9 Hz, ArH), 7.18−7.10 (m, 11H, ArH), 7.06 (t, 1H, $^3J_{HH}$ = 7.5 Hz, 7.3 ArH), 6.59 (dd, 2H, $^3J_{HP}$ = 10.3 Hz, $^3J_{HH}$ = 7.2 Hz, ArH), 4.39 (m, 2H, PCH_2N), 4.21 (dd, 2H, $^2J_{HH}$ = 14.5 Hz, $^2J_{HP}$ = 3.0 Hz, PCH_2N), 3.98 (d, 2H, $^2J_{HH}$ = 14.5 Hz, PCH_2N), 3.73 (m, 2H, PCH_2N), 3.21 (m, 2H, $P(CH_2)_2P$), 2.65 (m, 4H, $P(CH_2)_2P$), 2.49 (m, 2H, $P(CH_2)_2P$), 1.75 (s, 3H, CH_3CN), −21.2 (br s, $\Delta\nu_{1/2}$ = 144 Hz, 1H, CoH). ^{31}P{^{1}H} NMR (CD_3CN): δ 80 (br s, $\Delta\nu_{1/2}$ = 930 Hz, 2P), 76 (br s, $\Delta\nu_{1/2}$ = 1500 Hz, 2P). Anal. Calcd for $C_{46}H_{50}B_2CoF_8N_3P_4$: C, 55.17; H, 5.03; N, 4.20. Found: C, 54.53; H, 5.07; N, 4.47.

[HCo^{III}(L3)(CH$_3$CN)](BF$_4$)$_2$. This complex was prepared in a manner analogous to that described for $[HCo^{III}(L2)(CH_3CN)](BF_4)_2$ and was isolated as a yellow powder in 77% yield. The isolated product contained trace quantities of $[Co^{II}(L3)(CH_3CN)](BF_4)_2$ as determined by ^{1}H NMR spectroscopy. ^{1}H NMR (500 MHz, CD_3CN): δ 7.57 (t, 2H, $^3J_{HH}$ = 7.6 Hz, ArH), 7.49−7.37 (m, 6H, ArH), 7.27(t, 4H, $^3J_{HH}$ = 7.7 Hz, ArH), 7.24−7.11 (m, 13H, ArH), 7.07 (t, 1H, $^3J_{HH}$ = 7.3 Hz, ArH), 6.59 (dd, 2H, $^3J_{HP}$ = 9.7 Hz, $^3J_{HH}$ = 7.4 Hz, ArH), 4.24 (d, 2H, $^2J_{HH}$ = 14.6 Hz, PCH_2N), 4.01−3.87 (m, 6H, PCH_2N), 2.70 (m, 2H, $P(CH_2)_3P$), 2.48−2.27 (m, 4H, $P(CH_2)_3P$), 2.43 (s, CH_3CN), 2.20−2.00 (m, 6H, $P(CH_2)_3P$), −19.66 (p, 1H, $^2J_{HP}$ = 46.7 Hz, CoH). ^{31}P{^{1}H} NMR (CD_3CN): δ 21.8 (br s, $\Delta\nu_{1/2}$ = 234 Hz, 2P), 18.4 (br s, $\Delta\nu_{1/2}$ = 211 Hz, 2P). Anal. Calcd for $C_{48}H_{54}B_2CoF_8N_3P_4$: C, 56.00; H, 5.29; N, 4.08. Found: C, 55.54; H, 5.20; N, 4.18.

Bulk Electrolysis of [HCo^{III}(L2)(CH$_3$CN)](BF$_4$)$_2$. A three-necked 25 mL round-bottom flask was used as the bulk electrolysis vessel, and the electrolysis was performed in a glovebox. A 1 mm PEEK-encased glassy carbon electrode attached to copper wire was used as the working electrode for cyclic voltammogram measurements, and a cylinder of reticulated vitreous carbon attached to a copper wire was used as the working electrode for bulk electrolysis. The reference (silver wire) and counter electrode (Nichrome wire) were placed into 5 mm glass tubes terminating in Vycor fritted disks and filled with acetonitrile (0.2 M NEt_4BF_4). A solution of $[HCo^{III}(L2)(CH_3CN)](BF_4)_2$ (0.020 g, 0.020 mmol, 2 mM) and ferrocene (0.004 g, 0.02 mmol, 2 mM) in acetonitrile (0.2 M NEt_4BF_4, 10 mL) was transferred to the electrolysis vessel. Bulk electrolysis was performed at −1.81 V versus the ferrocenium/ferrocene internal reference until the current decreased to 4.5% of its initial value. A total of 2.0197 C of charge was passed, which corresponds to 1.1 mol of electrons per mole of $[HCo^{III}(L2)(CH_3CN)](BF_4)_2$. A cyclic voltammogram was recorded upon completion of the electrolysis, and an oxidation wave was observed at a potential corresponding to the $[Co^{II/I}(L2)(CH_3CN)]^{2+/+}$ couple.

Digital Simulations. DigiElch version 7.F (build 7.023) was used for digital simulations and nonlinear least-squares refinement of models against experimental data. Voltammograms were collected using a pre-equilibrium time of 2 s, and pre-equilibrium was enabled for all refinements. Background subtraction was employed for all data sets, and the double-layer capacitance (C_{dl}) was set to 0 for all refinements. A reasonable estimate for the solution resistivity, ρ (50 Ω), was made by manual iteration through comparison of the simulated and experimental E_p values for the $[Co^{II/I}(L2)(CH_3CN)]^{2+/+}$ couple, and this value was used for all refinements. Self-diffusion of acetonitrile was taken as 4.35×10^{-5} cm^2 s^{-1};[80] the activity of acetonitrile in the electrolyte solutions was taken to be 18 M, in accord with Tilset's estimate.[81] Current normalization was used for all refinements.

The diffusion coefficient (D_0) of $[Co^{II}(L2)(CH_3CN)]^{2+}$ was measured using chronoamperometry experiments and determined to be 9.6×10^{-6} cm^2 s^{-1} using the Cottrell equation, and this value was used for all cobalt species included in the digital simulations. Simulations of $[Co^{II}(L2)(CH_3CN)]^{2+}$ were performed on five voltammograms recorded from 1 to 50 V s^{-1} with an analyte concentration of 2 mM, and a heterogeneous electron transfer rate constant ($k°$) of 0.1 cm s^{-1} was obtained for this redox couple. In the experimental voltammograms of $[HCo^{III}(L2)(CH_3CN)]^{2+}$, a small amount of $[Co^{II}(L2)(CH_3CN)]^{2+}$ was observed as a contaminant on the initial cathodic sweep, and its bulk concentration was estimated to be 7% of the $[HCo^{III}(L2)(CH_3CN)]^{2+}$ concentration by manual iteration. A second unknown contaminant was observed at $E_{pc} \approx -1.1$

dx.doi.org/10.1021/ic401232g | Inorg. Chem. 2013, 52, 9975−9988

V and was not modeled since the concentration of this species was approximately 2% of the $[HCo^{III}(L2)(CH_3CN)]^{2+}$ concentration.

Three sets of refinements were performed for each monometallic and bimetallic reaction model: (1) free refinement on the 2 mM data set, (2) free refinement on the 1 mM data set, and (3) free refinement on the 1 mM data set with K_{eq} and k_{fwd} for reversible acetonitrile dissociation fixed to the values obtained from refinement on the 2 mM data set. Tables containing these refinement parameters are given in the Supporting Information. For refinement on the full data set, the heterogeneous electron transfer rate constant ($k°$) for all of the electron transfer steps was fixed initially at 0.1 cm s^{-1}. With $k°$ fixed, the simulated E_{pc} values were 40 mV positive of the experimental values at υ = 50 V s^{-1}, though better agreements were observed at lower scan rates. In subsequent refinements, $k°$ for the $[HCo^{II/I}(L2)]^{+/0}$ couple was allowed to refine freely, and $k°$ for the $[HCo^{III/II}(L2)(CH_3CN)]^{2+/+}$ couple was manually decreased until the experimental and simulated peak potentials differed by less than 15 mV at all scan rates.

X-ray Diffraction Studies. For each of the crystal structure studies, a single crystal grown from a CH_3CN solution layered with Et_2O was mounted using NVH immersion oil onto a nylon fiber and cooled to the data collection temperature of 100(2) K. Data were collected on a Bruker-AXS Kappa APEX II CCD diffractometer with 0.71073 Å Mo Kα radiation. Unit cell parameters were obtained from 90 data frames at 0.3° Φ from three different sections of the Ewald sphere. The data sets were treated with SADABS absorption corrections based on redundant multiscan data (Sheldrick, G., Bruker-AXS, 2001). All non-hydrogen atoms were refined with anisotropic displacement parameters. All hydrogen atoms were treated as idealized contributions except for the hydride ligand, which was located from the difference map and allowed to refine freely.

$[Co^{II}(L2)(CH_3CN)](BF_4)_2$. The systematic absences in the data were consistent with the centrosymmetric, monoclinic space group $P2_1/n$. The asymmetric unit contains one $[Co^{II}(L2)(CH_3CN)]^{2+}$ cation, two $[BF_4]^-$ anions and 2.5 molecules of acetonitrile solvent, all located on general positions yielding Z = 4 and Z' = 1. The $[BF_4]^-$ anions were disordered over two positions, which were located from the difference map and refined. The $[BF_4]^-$ bond lengths and angles were set equivalent to one another using the SAME command in an attempt to keep them chemically equivalent. A SQUEEZE analysis suggested 2.5 molecules of CH_3CN solvent per asymmetric unit. The difference map suggests three separate sites in the asymmetric unit for the acetonitrile. One is fully occupied and refines well. The other two are likely disordered over those two positions in a ratio that would lead to an average of 1.5 equiv of solvent. These did not refine well, and their geometries were bent instead of linear. Therefore, all three solvent molecules were removed using SQUEEZE. There was also two-part disorder in one of the phenyl rings of the ligand, which was located from the difference map and refined. The disordered rings were fixed using an AFIX66 command to help stabilize the refinement.

$[Co^{II}(L3)(CH_3CN)](BF_4)_2$. The data was consistent with the centrosymmetric, triclinic space group $P\bar{1}$. The asymmetric unit contains one $[Co^{II}(L3)(CH_3CN)]^{2+}$ cation, two $[BF_4]^-$ anions, and two molecules of acetonitrile solvent all located on general positions yielding Z = 2 and Z' = 1. There is two-part disorder in one of the BF_4^- anions, one phenyl ring, and one propyl bridge. In each case, the disorder was located from the difference map, and the two parts were restrained to be equivalent using the SAME command. SIMU and DELU commands were attempted to keep the thermal parameters of the disordered parts similar. However, these resulted in some NPD atoms in the disordered parts so more rigid EADP commands were used.

$[HCo^{III}(L2)(CH_3CN)](BF_4)_2$. The systematic absences in the data were consistent with the centrosymmetric, monoclinic space group $P2_1/c$. The asymmetric unit contains one $[HCo^{III}(L2)(CH_3CN)]^{2+}$ cation, two $[BF_4]^-$ anions, and one molecule of acetonitrile solvent all located on general positions yielding Z = 4 and Z' = 1. The thermal ellipsoid plot suggested that there was positional disorder in one of the phenyl rings; however, even after modeling and restraining the structure, the thermal parameters did not show significant improvement. Therefore, the modeling of this minor disorder was ignored in favor of a less-restrained model.

$[HCo^{III}(L3)(CH_3CN)](BF_4)_2$. The data was consistent with the centrosymmetric, triclinic space group $P\bar{1}$. The asymmetric unit contains one $[HCo^{III}(L3)(CH_3CN)]^{2+}$ cation, two $[BF_4]^-$ anions, and two molecules of acetonitrile solvent all located on general positions yielding Z = 2 and Z' = 1. There is two-part disorder in one of the $[BF_4]^-$ anions and one propyl bridge on the ligand. In each case, the disorder was located from the difference map and refined using SAME, SIMU, and DELU commands to keep the two parts similar.

■ ASSOCIATED CONTENT

Supporting Information

Experimental details of phosphine precursor synthesis, simulated $^{31}P\{^1H\}$ NMR spectrum of $[HCo^{III}(L2)(CH_3CN)]^{2+}$ and parameters, selected bond angles from X-ray diffraction, discussion of minor coordination isomers, calculation of predicted electron stoichiometry for a bulk electrolysis experiment, cyclic voltammetry plots, refinement parameters from digital simulation of cyclic voltammograms, and CIF files containing crystallographic data. This material is available free of charge via the Internet at http://pubs.acs.org.

■ AUTHOR INFORMATION

Corresponding Author

*E-mail addresses: eric.wiedner@pnnl.gov; morris.bullock@pnnl.gov.

Notes

The authors declare no competing financial interest.

■ ACKNOWLEDGMENTS

We thank the U.S. Department of Energy, Office of Basic Energy Sciences, Division of Chemical Sciences, Geosciences and Biosciences, for support of the initial parts of this study. Current work is supported by the Center for Molecular Electrocatalysis, an Energy Frontier Research Center funded by the U.S. Department of Energy, Office of Science, Office of Basic Energy Sciences. Pacific Northwest National Laboratory is operated by Battelle for the U.S. Department of Energy.

■ REFERENCES

(1) Lewis, N. S.; Nocera, D. G. *Proc. Natl. Acad. Sci. U. S. A.* **2006**, *103*, 15729−15735.
(2) Cook, T. R.; Dogutan, D. K.; Reece, S. Y.; Surendranath, Y.; Teets, T. S.; Nocera, D. G. *Chem. Rev.* **2010**, *110*, 6474−6502.
(3) Artero, V.; Chavarot-Kerlidou, M.; Fontecave, M. *Angew. Chem., Int. Ed.* **2011**, *50*, 7238−7266.
(4) Dempsey, J. L.; Brunschwig, B. S.; Winkler, J. R.; Gray, H. B. *Acc. Chem. Res.* **2009**, *42*, 1995−2004.
(5) Wang, M.; Chen, L.; Sun, L. *Energy Environ. Sci.* **2012**, *5*, 6763−6778.
(6) Lee, C. H.; Dogutan, D. K.; Nocera, D. G. *J. Am. Chem. Soc.* **2011**, *133*, 8775−8777.
(7) Marinescu, S. C.; Winkler, J. R.; Gray, H. B. *Proc. Natl. Acad. Sci. U. S. A.* **2012**, *109*, 15127−15131.
(8) Bigi, J. P.; Hanna, T. E.; Harman, W. H.; Chang, A.; Chang, C. J. *Chem. Commun.* **2010**, *46*, 958−960.
(9) Sun, Y.; Bigi, J. P.; Piro, N. A.; Tang, M. L.; Long, J. R.; Chang, C. J. *J. Am. Chem. Soc.* **2011**, *133*, 9212−9215.
(10) Singh, W. M.; Baine, T.; Kudo, S.; Tian, S.; Ma, X. A. N.; Zhou, H.; DeYonker, N. J.; Pham, T. C.; Bollinger, J. C.; Baker, D. L.; Yan, B.; Webster, C. E.; Zhao, X. *Angew. Chem., Int. Ed.* **2012**, *51*, 5941−5944.

(11) McNamara, W. R.; Han, Z.; Alperin, P. J.; Brennessel, W. W.; Holland, P. L.; Eisenberg, R. *J. Am. Chem. Soc.* **2011**, *133*, 15368−15371.
(12) Razavet, M.; Artero, V.; Fontecave, M. *Inorg. Chem.* **2005**, *44*, 4786−4795.
(13) Hu, X. L.; Cossairt, B. M.; Brunschwig, B. S.; Lewis, N. S.; Peters, J. C. *Chem. Commun.* **2005**, 4723−4725.
(14) Baffert, C.; Artero, V.; Fontecave, M. *Inorg. Chem.* **2007**, *46*, 1817−1824.
(15) Jacques, P. A.; Artero, V.; Pecaut, J.; Fontecave, M. *Proc. Natl. Acad. Sci. U. S. A.* **2009**, *106*, 20627−20632.
(16) Hu, X. L.; Brunschwig, B. S.; Peters, J. C. *J. Am. Chem. Soc.* **2007**, *129*, 8988−8998.
(17) McCrory, C. C. L.; Uyeda, C.; Peters, J. C. *J. Am. Chem. Soc.* **2012**, *134*, 3164−3170.
(18) Stubbert, B. D.; Peters, J. C.; Gray, H. B. *J. Am. Chem. Soc.* **2011**, *133*, 18070−18073.
(19) Berben, L. A.; Peters, J. C. *Chem. Commun.* **2010**, *46*, 398−400.
(20) Valdez, C. N.; Dempsey, J. L.; Brunschwig, B. S.; Winkler, J. R.; Gray, H. B. *Proc. Natl. Acad. Sci. U. S. A.* **2012**, *109*, 15589−15593.
(21) Du, P.; Schneider, J.; Luo, G.; Brennessel, W. W.; Eisenberg, R. *Inorg. Chem.* **2009**, *48*, 4952−4962.
(22) Lazarides, T.; McCormick, T.; Du, P.; Luo, G.; Lindley, B.; Eisenberg, R. *J. Am. Chem. Soc.* **2009**, *131*, 9192−9194.
(23) Du, P.; Eisenberg, R. *Energy Environ. Sci.* **2012**, *5*, 6012−6021.
(24) Zhang, P.; Jacques, P. A.; Chavarot-Kerlidou, M.; Wang, M.; Sun, L.; Fontecave, M.; Artero, V. *Inorg. Chem.* **2012**, *51*, 2115−2120.
(25) Probst, B.; Rodenberg, A.; Guttentag, M.; Hamm, P.; Alberto, R. *Inorg. Chem.* **2010**, *49*, 6453−6460.
(26) Probst, B.; Guttentag, M.; Rodenberg, A.; Hamm, P.; Alberto, R. *Inorg. Chem.* **2011**, *50*, 3404−3412.
(27) Li, L.; Duan, L.; Wen, F.; Li, C.; Wang, M.; Hagfeldt, A.; Sun, L. *Chem. Commun.* **2012**, *48*, 988−990.
(28) Huang, J.; Mulfort, K. L.; Du, P.; Chen, L. X. *J. Am. Chem. Soc.* **2012**, *134*, 16472−16475.
(29) Hawecker, J.; Lehn, J. M.; Ziessel, R. *New J. Chem.* **1983**, *7*, 271−277.
(30) Fihri, A.; Artero, V.; Pereira, A.; Fontecave, M. *Dalton Trans.* **2008**, 5567−5569.
(31) Fihri, A.; Artero, V.; Razavet, M.; Baffert, C.; Leibl, W.; Fontecave, M. *Angew. Chem., Int. Ed.* **2008**, *47*, 564−567.
(32) Solis, B. H.; Hammes-Schiffer, S. *Inorg. Chem.* **2011**, *50*, 11252−11262.
(33) Dempsey, J. L.; Winkler, J. R.; Gray, H. B. *J. Am. Chem. Soc.* **2010**, *132*, 16774−16776.
(34) King, A. E.; Surendranath, Y.; Piro, N. A.; Bigi, J. P.; Long, J. R.; Chang, C. J. *Chem. Sci.* **2013**, *4*, 1578−1587.
(35) Muckerman, J. T.; Fujita, E. *Chem. Commun.* **2011**, *47*, 12456−12458.
(36) Schrauzer, G. N.; Holland, R. J. *J. Am. Chem. Soc.* **1971**, *93*, 1505−1506.
(37) Bhattacharjee, A.; Chavarot-Kerlidou, M.; Andreiadis, E. S.; Fontecave, M.; Field, M. J.; Artero, V. *Inorg. Chem.* **2012**, *51*, 7087−7093.
(38) Rahman, A. F. M. M.; Jackson, W. G.; Willis, A. C.; Rae, A. D. *Chem. Commun.* **2003**, 2748−2749.
(39) Wiedner, E. S.; Yang, J. Y.; Dougherty, W. G.; Kassel, W. S.; Bullock, R. M.; DuBois, M. R.; DuBois, D. L. *Organometallics* **2010**, *29*, 5390−5401.
(40) Jacobsen, G. M.; Yang, J. Y.; Twamley, B.; Wilson, A. D.; Bullock, R. M.; DuBois, M. R.; DuBois, D. L. *Energy Environ. Sci.* **2008**, *1*, 167−174.
(41) Wiedner, E. S.; Yang, J. Y.; Chen, S. T.; Raugei, S.; Dougherty, W. G.; Kassel, W. S.; Helm, M. L.; Bullock, R. M.; DuBois, M. R.; DuBois, D. L. *Organometallics* **2012**, *31*, 144−156.
(42) King, R. B.; Cloyd, J. C.; Kapoor, P. N. *J. Chem. Soc., Perkin Trans. 1* **1973**, 2226−2229.
(43) Meier, U. W.; Hollmann, F.; Thewalt, U.; Klinga, M.; Leskelä, M.; Rieger, B. *Organometallics* **2003**, *22*, 3905−3914.
(44) Garrou, P. E. *Chem. Rev.* **1981**, *81*, 229−266.
(45) Kilgore, U. J.; Roberts, J. A. S.; Pool, D. H.; Appel, A. M.; Stewart, M. P.; DuBois, M. R.; Dougherty, W. G.; Kassel, W. S.; Bullock, R. M.; DuBois, D. L. *J. Am. Chem. Soc.* **2011**, *133*, 5861−5872.
(46) Galan, B. R.; Schöffel, J.; Linehan, J. C.; Seu, C.; Appel, A. M.; Roberts, J. A. S.; Helm, M. L.; Kilgore, U. J.; Yang, J. Y.; DuBois, D. L.; Kubiak, C. P. *J. Am. Chem. Soc.* **2011**, *133*, 12767−12779.
(47) Kilgore, U. J.; Stewart, M. P.; Helm, M. L.; Dougherty, W. G.; Kassel, W. S.; DuBois, M. R.; DuBois, D. L.; Bullock, R. M. *Inorg. Chem.* **2011**, *50*, 10908−10918.
(48) Ciancanelli, R.; Noll, B. C.; DuBois, D. L.; DuBois, M. R. *J. Am. Chem. Soc.* **2002**, *124*, 2984−2992.
(49) Mock, M. T.; Potter, R. G.; O'Hagan, M. J.; Camaioni, D. M.; Dougherty, W. G.; Kassel, W. S.; DuBois, D. L. *Inorg. Chem.* **2011**, *50*, 11914−11928.
(50) Bard, A. J.; Faulkner, L. R. *Electrochemical Methods: Fundamentals and Applications*, 2nd ed.; John Wiley & Sons: Hoboken, NJ, 2001.
(51) Nicholson, R. S.; Shain, I. *Anal. Chem.* **1964**, *36*, 706−723.
(52) Savéant, J. M. *Elements of Molecular and Biomolecular Electrochemistry: An Electrochemical Approach to Election Transfer Chemistry*; Wiley: Hoboken, NJ, 2006.
(53) Koelle, U.; Ohst, S. *Inorg. Chem.* **1986**, *25*, 2689−2694.
(54) Krafft, M. J.; Bubrin, M.; Paretzki, A.; Lissner, F.; Fiedler, J.; Záliš, S.; Kaim, W. *Angew. Chem., Int. Ed.* **2013**, *52*, 6781−6784.
(55) Nimlos, M. R.; Chang, C. H.; Curtis, C. J.; Miedaner, A.; Pilath, H. M.; DuBois, D. L. *Organometallics* **2008**, *27*, 2715−2722.
(56) Berning, D. E.; Miedaner, A.; Curtis, C. J.; Noll, B. C.; DuBois, M. C. R.; DuBois, D. L. *Organometallics* **2001**, *20*, 1832−1839.
(57) Berning, D. E.; Noll, B. C.; DuBois, D. L. *J. Am. Chem. Soc.* **1999**, *121*, 11432−11447.
(58) Raebiger, J. W.; Miedaner, A.; Curtis, C. J.; Miller, S. M.; Anderson, O. P.; DuBois, D. L. *J. Am. Chem. Soc.* **2004**, *126*, 5502−5514.
(59) Wayner, D. D. M.; Parker, V. D. *Acc. Chem. Res.* **1993**, *26*, 287−294.
(60) Parker, V. D.; Handoo, K. L.; Roness, F.; Tilset, M. *J. Am. Chem. Soc.* **1991**, *113*, 7493−7498.
(61) Tilset, M.; Parker, V. D. *J. Am. Chem. Soc.* **1990**, *112*, 2843−2843.
(62) Tilset, M.; Parker, V. D. *J. Am. Chem. Soc.* **1989**, *111*, 6711−6717.
(63) Tilset, M. *J. Am. Chem. Soc.* **1992**, *114*, 2740−2741.
(64) Skagestad, V.; Tilset, M. *J. Am. Chem. Soc.* **1993**, *115*, 5077−5083.
(65) Roberts, J. A. S.; Appel, A. M.; DuBois, D. L.; Bullock, R. M. *J. Am. Chem. Soc.* **2011**, *133*, 14604−14613.
(66) Tilset, M.; Hamon, J. R.; Hamon, P. *Chem. Commun.* **1998**, 765−766.
(67) Raebiger, J. W.; DuBois, D. L. *Organometallics* **2005**, *24*, 110−118.
(68) Miedaner, A.; Raebiger, J. W.; Curtis, C. J.; Miller, S. M.; DuBois, D. L. *Organometallics* **2004**, *23*, 2670−2679.
(69) Chen, S.; Rousseau, R.; Raugei, S.; Dupuis, M.; DuBois, D. L.; Bullock, R. M. *Organometallics* **2011**, *30*, 6108−6118.
(70) Appel, A. M.; Lee, S. J.; Franz, J. A.; DuBois, D. L.; DuBois, M. R. *J. Am. Chem. Soc.* **2009**, *131*, 5224−5232.
(71) Pleune, B.; Morales, D.; Meunier-Prest, R.; Richard, P.; Collange, E.; Fettinger, J. C.; Poli, R. *J. Am. Chem. Soc.* **1999**, *121*, 2209−2225.
(72) Pleune, B.; Poli, R.; Fettinger, J. C. *J. Am. Chem. Soc.* **1998**, *120*, 3257−3258.
(73) Bianchini, C.; Laschi, F.; Peruzzini, M.; Ottaviani, F. M.; Vacca, A.; Zanello, P. *Inorg. Chem.* **1990**, *29*, 3394−3402.
(74) Heinekey, D. M.; Liegeois, A.; Vanroon, M. *J. Am. Chem. Soc.* **1994**, *116*, 8388−8389.
(75) Hathaway, B. J.; Holah, D. G.; Underhill, A. E. *J. Chem. Soc.* **1962**, 2444−2448.

(76) Heintz, R. A.; Smith, J. A.; Szalay, P. S.; Weisgerber, A.; Dunbar, K. R. *Inorg. Synth.* **2002**, *33*, 75−83.
(77) Evans, D. F. *J. Chem. Soc.* **1959**, 2003−2005.
(78) Schubert, E. M. *J. Chem. Educ.* **1992**, *69*, 62−62.
(79) Baker, M. V.; Field, L. D.; Hambley, T. W. *Inorg. Chem.* **1988**, *27*, 2872−2876.
(80) Hurle, R. L.; Woolf, L. A. *J. Chem. Soc., Faraday Trans. 1* **1982**, *78*, 2233−2238.
(81) Tilset, M. *Inorg. Chem.* **1994**, *33*, 3121−3126.